DEUTSCHES ELEKTRONEN-SYNCHROTRON DESY

DESY 81/037
July 1981

RECENT EXPERIMENTAL RESULTS IN $\gamma\gamma$ INTERACTIONS

by

J. H. Field

NOTKESTRASSE 85 · 2 HAMBURG 52

To be sure that your preprints are promptly included in the
HIGH ENERGY PHYSICS INDEX ,
send them to the following address (if possible by air mail) :

DESY
Bibliothek
Notkestrasse 85
2 Hamburg 52
Germany

DESY 81/037
July 1981

RECENT EXPERIMENTAL RESULTS IN $\gamma\gamma$ INTERACTIONS

J.H. Field

Deutsches Elektronen-Synchrotron DESY, Hamburg

Rapporteur talk at the International Colloquium on
Photon Photon Interactions,
6. - 9.4.1981, Paris

Summary of the Experimental Discussion Session

In the experimental discussion session 7 short talks were presented. The speakers and their subjects were:

S. Kawabata:	(JADE Collaboration)	A new general Monte Carlo event generator
H. Kolanoski:	(TASSO Collaboration)	$\rho\rho$ production
J. Olsson:	(JADE Collaboration)	$\eta' \to \rho\gamma$
K. Wacker:	(Crystal Ball)	$f_0 \to \pi^0\pi^0$, $A_2 \to \eta^0\pi^0$
J.H. Field:	(CELLO Collaboration)	$f_0 \to \pi^+\pi^-$
P. Leu:	(TASSO Collaboration)	$f_0 \to \pi^+\pi^-$, $S_0 \to \pi^+\pi^-$
N. Wermes:	(TASSO Collaboration)	Evidence for hard processes in $\gamma\gamma$ interactions

I shall try as far as possible to confine myself to the material actually presented in the session, though in the case of f_0 production, and the important new evidence for hard subprocesses in $\gamma\gamma$ collisions where I attempt a general survey of new data first shown at this conference some overlap with other Rapporteurs (Burke, Hilger, and Cords) is inevitable. I particularly emphasise special and (to me) interesting points that were raised in the discussion session, which because of time pressure were touched on only briefly by the other speakers. I make no attempt to give a comprehensive list of cross sections, $\gamma\gamma$ widths of resonances etc. For this the reader is referred to the talks of the other Rapporteurs.

Kawabata

Particularly in the calculation of the QED process

$$ee \to eel^+l^- \quad (l = \text{lepton})$$

it has been customary to use programs containing the exact matrix element of the lowest order Feynman diagram, thus avoiding all uncertainties due to various approximate formulae which use the equivalent photon approximation, or contain only the contribution of transverse virtual photons. The most widely used program of this type is that of Vermaseren.

A more recent program using a similar philosophy is that of Vermaseren and Krasemann[1] for the processes:

$$ee \to ee \begin{cases} f_0 \\ \mu^+\mu^- \end{cases}$$

where detailed quark model amplitudes are included. All of these programs use the technique of Monte Carlo integration. Cuts are applied to correspond to experimental acceptance limitations. Mass distributions, angular distributions etc. are then directly generated. This implies that the program must be re-run if a different set of cuts is applied or different distributions are required. For many experimental applications (for example to properly include the effects of detector resolution and efficiency on the distributions) it is preferable to generate actual Monte Carlo events (i.e. 4 vectors of particles) with unit weight. Because of the extreme peakiness of the angular distributions in the $\gamma\gamma$ processes, following from the effects of the virtual photon propagators, it is difficult to do this with a high efficiency ε where:

$$\varepsilon = \frac{\text{number of accepted events}}{\text{number of trials}}$$

The problem is illustrated for a simple one dimensional case in Fig. 1. If points are thrown uniformly within the box shown in Fig. 1a ε is about 50%. If however the intervals along the x-axis are chosen as in Fig. 1b and points are thrown with equal probability into these intervals the distribution is generated with an efficiency near 100%.

This is the technique used by Kawabata to generate an arbitrary distribution function:

$$\frac{d^N\sigma}{dx_1 \ldots dx_N} = f(x_1, \ldots x_N) \quad , \; 1 \leq N \leq 10$$

The generation is done in 5 steps

(I) The integration program VEGAS (written by P. Lepage) is used to search for optimum sampling intervals of the function f in the N dimensional parameter space

(II) Using a number of adjacent intervals in each parameter the space is divided up into groups of hypercubes. The probabilities and sampling intervals for these groups are stored on disc (for the 7 parameters needed for the $ee \to ee\ell^+\ell^-$ differential cross-section there are 2187 such groups)

(III) A group is chosen according to the stored probability

(IV) A hypercube is chosen within the group

(V) A point is chosen within the hypercube. f is calculated at this point and its value compared with the maximum within the group. Then

$$\text{reject} \quad \text{if} \quad \frac{f}{f_{MAX}} \; \begin{cases} < \\ > \end{cases} \; \begin{cases} \text{Random number} \\ \end{cases} \quad \text{accept}$$

'Reject' means return to step (IV) and repeat; 'accept' store the generated event.

The program has been used to generate the processes:

a) $ee \to ee\ell^+\ell^-$ (N = 7)
b) $ee \to eeX$ (N = 5)

Comparisons of the histograms of generated events with distributions given by Vermaseren's program for two typical angular distributions for process a) are shown in Fig. 2. Fig. 3 shows a comparison for process b) with curves for the total and doubly tagged luminosity functions appearing in Ref. (1). In this last case Monte Carlo integration is used directly to give the points shown.

The speed of event generation is high: 130 events/sec, 1000 events/sec for processes a), b) respectively on the DESY IBM computer.

Within the last year another event generator written specificly for 2 photon reactions has been developed within the CELLO collaboration by A. Snyder and the author. It can be used to generate an arbitrary $\gamma\gamma$ process using the exact transverse luminosity function. A similar idea of dividing up the parameter space into regions with pre-calculated integrated probabilities was used. For the process $ee \to ee\ell^+\ell^-$ $\sim$ 170 events/sec are generated on the DESY IBM. As the program uses lab. angles, rather than the Q^2 of the virtual photons as variables the efficiency of generation of tagged cross sections in fixed angular ranges is high.

Kolanoski

Kolanoski presented data on the reaction

$$ee \to 2\pi^+ 2\pi^- ee$$

as observed in the TASSO detector. The integrated luminosity was 8585 nb^{-1} and the beam energy was in the range 15-18.3 GeV. No tagging was used.

Evidence for the production of 4 charged pions by the two photon process is shown in Figs. 4 and 5. Fig. 4 shows the distribution of $(\sum_i \vec{p}_T^{\,i})^2$ where $\vec{p}_T^{\,i}$ is the momentum component of track i transverse to the beams. Fig. 5 shows $\sum_i p_x^i$ plotted against $\sum_i p_y^i$ where x and y are two orthogonal axes perpendicular to the beams. The peaking at low $(\sum \vec{p}_T)^2$ for events produced by the two photon mechanism is evident. In Fig. 4 the estimated level of background under the 2γ production peak is indicated. The sharp peaking in $(\sum \vec{p}_T)^2$ shows that the exclusive 4 charged pion channel is indeed observed. The dominance of this channel by the reaction $\gamma\gamma \to \rho^0\rho^0$ is shown clearly in Fig. 6 where the opposite sign dipion mass combinations (two entries per event) are shown on a scatter plot. A strong peaking can be seen where two mass combinations are both in the region of the ρ^0. In contrast the scatter plot of equal sign mass combinations (one entry per event) shows no such structure (Fig. 7). Details of the fit to the hypotheses $\rho^0\rho^0$, $\rho^0\pi^+\pi^-$ and 4π phase space are given in Hilger's talk. Here we focus instead firstly on the question of the correct form of the distribution function to be used to describe the $\rho^0\rho^0$ channel, and secondly on the interpretation of the large $\rho^0\rho^0$ cross section which is observed just above threshold for the process.

As has been pointed out by A. Courau[3], in the region near threshold for the reaction $\gamma\gamma \to \rho^0\rho^0$, there is a good probability that all 4 possible opposite sign mass combinations for a given event will lie within the ρ^0 resonance region. In this case it is important to use a properly symmetrised form for the production amplitude and to add the two symmetrised amplitudes before squaring to find the cross section. Denoting the 4 pions by π_1^+, π_2^-, π_3^+, π_4^- the cross section then takes the form:

$$\sigma_{sym}^{\gamma\gamma\to\rho\rho} \propto |A(M_{12})A(M_{34})W(\cos\theta_{12}) + A(M_{13})A(M_{24})W(\cos\theta_{13})|^2$$

where A is a Breit-Wigner amplitude, and W is the angular distribution function of $\gamma\gamma \to \rho\rho$ in the $\gamma\gamma$ CM frame. Tentative evidence that this symmetrised form is indeed required to fit the TASSO data is shown in Fig. 8 where the mean mass per event of the $\pi\pi$ combinations is shown. The mean $\pi\pi$ mass combinations for opposite sign (solid histogram) and same sign (dotted histogram) pion pairs are shown in Fig. 8a. Monte Carlo distributions using a non symmetrised and a symmetrised distribution function respectively are shown in Figs. 8b and 8c. Taking the fraction of combinations in the mass region $M_{\pi\pi}<0.6$ GeV for the 3 distributions leads to the results:

	Data	Non-Sym.M.C.	Sym. M.C.
Opp. sign pairs	16±3%	24%	20%
Same sign pairs	47±7%	35%	43%

The symmetrised function seems favoured, fitting the data perfectly; whereas the non symmetrised function requires a statistical fluctuation $\gtrsim 2\,\sigma$ to explain the data.

The problem of the interpretation of the large $\rho^0\rho^0$ cross section remains largely open, though the new data from the MARK II detector at SPEAR (see the talk of D. Burke) makes unlikely the narrow resonance interpretation advanced by some authors[4],[5] on the basis of the early TASSO data. The lower mass points now available from MARK II lie well above the fits to the TASSO data found in Ref (3) and (4) (see the talk of P. Landshoff). The cleanest way, presumably, to rule out or establish a resonance interpretation of the peak is to look for the $\rho^+\rho^-$ signal, which by isospin should have double the cross section for $\rho^0\rho^0$, assuming the resonance is an iso-singlet. However exclusive measurement of $\rho^+\rho^-$ requires the detection of 4 γ s implying large angle coverage with electromagnetic shower detectors. At PETRA the CELLO and JADE detectors seem best suited to look for this channel. Table 1, presented by Kolanoski, shows the expected cross section ratios for the channels $\rho^0\rho^0$, $\rho^+\rho^-$, $\omega^0\omega^0$, $\rho^0\omega^0$ for 4 different models of the production process. Krammer[6] and Biswal and Misra[7] use different types of quark recombination model.

In Krammer's model the quark charges are counted only at the photon vertices, whereas in the model of Biswal and Misra they are also counted when the quarks recombine to produce the observed vector mesons. In any case at high masses (say $M_{\rho\rho} \gtrsim 10$ GeV) the naive VDM model of $\rho\rho$ scattering is expected to emerge, with strong backward-forward peaking of the produced ρ's and a $\sin^2\theta_H$ decay distribution following from helicity

conservation. There is evidence already in the high mass data from TASSO that the exclusive 4π production cross section is already consistent with the VDM (factorisation) value.

Olsson

The data presented by Olsson on the process

$$ee \to ee\eta' \qquad \text{(untagged)}$$
$$\eta' \to \rho^0\gamma$$
$$\rho^0 \to \pi^+\pi^-$$

highlights two strong points of the JADE detector:

- good particle identification capability
- detection of electromagnetic showers with good efficiency (above 300 MeV the detection efficiency approaches 100%) and good angular and energy resolution.

Fig. 9 shows the $\pi^+\pi^-$ and $\pi^+\pi^-\gamma$ mass spectra seen in JADE for a sample of events with 1 and only 1 γ observed in association with two oppositely charged tracks. At this stage there is no identification of the pions, but a clear peak can be seen in the region of the ρ^0 in the $\pi^+\pi^-$ spectrum, and in the region of the η' in the $\pi^+\pi^-\gamma$ spectrum. Using the dE/dx measurement in the JET detector pions are clearly separated from electrons in the momentum range of interest here (Fig. 10). Rejecting the electrons using the dE/dx measurement leads to much improved signal/background ratios for both the ρ^0 and the η' signal (Figs. 11, 12). Cutting on the ρ^0 mass region $600<M(\pi^+\pi^-)<900$ MeV retains almost all events in the η' peak (shaded histogram, Fig. 12) so the decay $\eta'\to\pi^+\pi^-\gamma$ is consistent with the hypothesis that it proceeds almost 100% via the $\rho^0\gamma$ channel.

The production cross section, calculated at an average beam energy of 16.7 GeV is

$$\sigma_{TOT}(ee\to ee\eta') = 3.1\pm0.7 \text{ nb (statistical error only)}$$

The corresponding radiative width, using the formula of Brodsky, Kinoshita and Terazawa[8] is

$$\Gamma^{\eta'}_{\gamma\gamma} = 7.5\pm1.7 \text{ keV (statistical error only)}$$

to be compared with the measurement from MARK II at SPEAR[9]

$$\Gamma^{\eta'}_{\gamma\gamma} = 5.8\pm1.1\pm1.2$$

where, as below, the first error quoted is statistical, the second systematic.

Wacker

Although the results from the Crystal Ball - by general consensus, the most beautiful in a purely experimental sense, presented at this Conference - have already been covered in some detail in Burke's talk I should like to go over them again here. First and foremost because they are so beautiful, and secondly because of their relevance to the discussion of the structure in and around the f_0 peak and of possible mass shifts of the f_0 from the 'data book' value of 1273 MeV/c^2[10].

Fig. 13 shows the geometrical structure of the 'Crystal Ball' - a matrix of NaI counters of triangular cross section forming an almost complete spherical shell. Charged particles are detected in cylindrical track chambers, but there is no magnetic analysis of charged momenta. The data described here has 4 detected γ's in the final state and no charged particles. The distribution of energy over the NaI counters in a 4γ event is shown in Fig. 14. The 4 clusters of energy corresponding to the detected γ's are clearly visible and there is no background in the detector.

On plotting the invariant mass of the 4γ system a broad peak is observed in the mass region

$$1000<M(4\gamma)<1500 \text{ MeV}/c^2 \text{ (see the talk of D. Burke)}$$

On making a cut on the 4γ mass

$$1040<M(4\gamma)<1500 \text{ MeV}/c^2$$

and on the total transverse momentum of the 4 γ's (to select $\gamma\gamma$ production events)

$$p_T^2 < 0.03 \text{ GeV}/c^2$$

the plot shown in Fig. 15 is obtained, where the high $\gamma\gamma$ mass combination is plotted against the low one (3 combinations per event).
Clear structures are evident in the $\pi^0\pi^0$ and $\pi^0\eta^0$ regions. Taking events in the $\pi^0\pi^0$ band and subtracting the combinatorial background gives the $\pi^0\pi^0$ mass spectrum shown in Fig. 16. There is a clean background-free f_0 peak but the central value of 1213 MeV is below the data book value by $\sim$ 60 MeV. Fig. 17 is as Fig. 16 except that the data has a lower trigger-threshold. A

similar mass shift is observed. Because the virtual photon luminosity function favours small masses some mass shift of a perfectly symmetrical resonance towards smaller values is expected if the line shape is not corrected for the luminosity function. This effect is shown in Fig. 18 where the expected $\pi^0\pi^0$ spectrum for an f_0 of mass 1270 MeV/c^2 is shown - there is a shift of 30 MeV/c^2 from this effect. The remaining effect, a 2-3% shift, is much larger than the uncertainty in the calibration of the NaI counters and is almost certainly a real effect. As evidence that the calibration is correct, Fig. 19 shows the $\gamma\gamma$ mass distribution in the region of the π^0 mass peak - the correct value for M_{π^0} is obtained within a fraction of a percent.

Fig. 20 shows the decay angular distribution of the f_0 in its rest frame relative to the beam direction. The fitted contribution of the helicity 2, 1, 0 states are shown. The f_0 is clearly in an almost pure helicity 2 state as expected from theoretical considerations[11]. The measurement of the helicity state is made possible by the background free nature of the f_0 sample and the good angular acceptance of the crystal ball. Knowledge of the helicity state is extremely important for the determination of $\Gamma_{\gamma\gamma}^{f_0}$. Cutting at $|\cos\theta|<0.8$ for the $\pi^+\pi^-$ decay mode for example gives an experimental acceptance $\sim$ 2 times higher for the $\lambda=2$ than for the $\lambda=0$ state at typical PETRA energies. The value for $\Gamma_{\gamma\gamma}^{f_0}$ quoted in Burke's talk is the first experimental measurement free from uncertainties due to the helicity structure of the f_0 decay.

Fig. 21 shows the high versus low $\gamma\gamma$ mass combinations after removing the $\pi^0\pi^0$ events. The much reduced combinatorial background makes even more evident the $\pi^0\eta^0$ signal. The $\pi^0\eta^0$ mass spectrum (Fig. 22) shows a clear background free signal for the A_2 as well as some structure of marginal statistical significance around 1 GeV/c^2.

Assuming the A_2 is also in the helicity 2 state the following value for $\Gamma_{\gamma\gamma}^{A_2}$ is found:

$$\Gamma_{\gamma\gamma}^{A_2} = 0.77 \pm 0.18 \pm 0.27 \text{ keV}$$

These beautiful results from a small highly specialised detector show that the 'measure everything' philosophy of the typical experimental

set up at e^+e^- machines does not always produce the best results and that the physics capabilities of high precision calorimeters such as the Crystal Ball extend well beyond the more obvious fields of applicability - QED processes and heavy quarkonium studies.

Field

This conference has seen the first, preliminary, results on 2γ physics from the new CELLO detector at PETRA. The strong point of CELLO for this type of physics is the low bias of its charged particle trigger against final states with small visible energy. This is largely made possible by the reduction of background trigger rate from cosmics and beam gas interactions by a factor of 10 or more by the 'RZ' trigger. This trigger, unique among detectors at PETRA, rejects all events not originating from a distance $\sim \pm$ 10 cm from the interaction point along the beam. The trigger condition used for the untagged data presented here required 2 tracks of transverse momenta > 200 MeV in the bending plane (without angular restrictions) and one track in a plane containing the beam. The resulting good low mass acceptance is shown in Figs. 23 and 24. Fig. 24 is the mass spectrum (assuming the particles to be pions) of events with two charged tracks of opposite sign observed in the detector at angles to the beam such that $|\cos\theta|<0.7$ and $p_T>250$ MeV/c for both tracks. After a cut on collinear events to remove cosmic muons vertex plots indicate a background level $\sim$1%. No attempt at $\pi/\mu/e$ discrimination is made. A clear f_0 signal is seen as well as some tentative evidence for S^* (980).
In the scatter plot of 2 body mass against the total transverse momentum of the pair (Fig. 24) the f_0 events are seen to be concentrated at low p_T^{PAIR}, whereas at lower masses there is perhaps evidence for an 'inclusive ρ' signal coming from higher multiplicity events where one or more tracks or neutral energy escapes detection. In this preliminary data no use is made of information from the liquid argon calorimeters. However first studies indicate that electrons can be reliably identified using the liquid argon calorimeters for electron energies greater than 500 MeV/c - and this will be used in further analysis to reduce the QED background under the resonant peaks. Fig. 25 shows the f_0 signal after subtraction of a Monte Carlo estimate of the QED background. The normalisation of this background is somewhat uncertain as can be seen in Fig. 23. The Monte Carlo curve ($ee\gamma\mu\mu$)

containing no correction for experimental resolution and matched to the data only by the p_T and cosθ cuts given above fits rather poorly in the low mass interval. If it is normalised to the data in the mass interval 0.55-0.85 GeV/c^2 (I) it gives a poor fit in the interval 0.55-0.7 GeV/c^2 (Ia) being too high there and too low in the interval 0.7-0.55 GeV c^2 (Ib). Normalising in Region (I) as for the subtracted spectrum of Fig. 25 gives a good fit in the high mass tail 1.5-2.0 GeV/c^2. This region has however poor statistical sensitivity. The main systematic uncertainty in the determination $\Gamma^{f_0}_{\gamma\gamma}$ comes from this normalisation uncertainty. The value:

$$\Gamma^{f_0}_{\gamma\gamma} = 2.41 \pm 0.17 \pm 0.51 \text{ keV} \quad (\lambda = 2 \text{ assumed})$$

is given by taking the normalisation in interval I to give the central value, and that in interval Ia, Ib giving respectively low, high background under the f_0 to estimate the range of systematic error. This estimate of the background subtraction error is conservative, however there is a further systematic error, not quoted above, due to the effect of finite experimental resolution on the acceptance. As the cross section for f_0 production is calculated by normalising to the observed number of QED events ($ee+\mu\mu$) the quoted value of $\Gamma^{f_0}_{\gamma\gamma}$ is independant of absolute normalisation, trigger efficiency and track reconstruction efficiency which should be identical for the f_0 and QED events.

Leu

The best high energy data on f_0 production presented here came from the TASSO collaboration. With an integrated luminosity of 9240 nb^{-1} in the range of beam energy from13.7-18.3 Gevthey observed ∿ 1556 events above background in the f_0 mass region. Fig. 26 shows the unsubtracted $\pi^+\pi^-$ mass spectrum. The acceptance is good for the f_0 itself but drops rapidly below masses of 1 GeV/c^2. The QED background curve, generated using the Vermaseren program and including ee and μμ production is normalised to the high mass tail $M_{\pi^+\pi^-} > 2.0$ GeV/c^2. Fig.27 shows the $\pi^+\pi^-$ spectrum after subtraction of the QED background. A fit is shown putting in 'data book'[10] values for the f_0 and $S^*(980)$ position and width. The S^* seems to be required by the data, however the detector acceptance is falling fast on the low mass side of this bump, and there is some inconsistency here between the 4 experiments with data on $f_0 \to \pi^+\pi^-$, TASSO, CELLO, JADE and MARK II. This is discussed in more detail below. It can be seen in Fig. 27 that the f_0 mass peak is shifted to

lower values, and also the width is somewhat larger than the data book value. Allowing a free fit to the parameters of the f_0 and S^* leads to the results:

		Data book values
M_{f_0}	= 1250 ± 7 MeV	1273 ± 5
Γ_{f_0}	= 210 ± 20 MeV	178 ± 20
M_{S^*}	= 990 ± 20 MeV	980 ± 10
Γ_{S^*}	= 50 ± 20 MeV	40 ± 10

Although the agreement for the S^* parameters is satisfactory there are possibly significant shifts of M_{f_0}, Γ_{f_0}. The broadening of the f_0 peak is hardly statistically significant, but there is some evidence (as in the MARK II and CELLO data) for a downward shift of the mass. With a contribution from the possible decay $f' \to K^+K^-$ (K^+, K^- are assigned the pion mass) there is some improvement in the fit, as shown in Fig. 28. If the data is interpreted in this way the following radiative widths are found, taking data book values for the resonance masses and widths:

$$\Gamma^{f_0}_{\gamma\gamma} = 3.2 \pm 0.2 \pm 0.6 \text{ keV (Helicity 2 assumed)}$$

$$\Gamma^{f'}_{\gamma\gamma} \times BR(f' \to K^+K^-) \leq 1.3 \text{ keV (95\% C.L., Helicity 2 assumed)}$$

$$\Gamma^{S^*}_{\gamma\gamma} \times BR(S^* \to \pi^+\pi^-) = 1.3 \pm 0.4 \pm 0.6 \text{ keV}$$

Fig. 29 shows the subtracted centre of mass decay angular distribution (with respect to the beam direction) for the f_0 peak. The λ=2 helicity state is seen to be favoured.

TASSO also has data on f_0 production in the single tag mode. The unsubtracted and subtracted distributions are shown in Fig. 30. The f_0 signal is perhaps not statistically significant. For the single tagged data it is found that:

$$\Gamma^{f_0}_{\gamma\gamma} = 1.6 \pm 0.6 \pm 0.3 \text{ keV (Helicity state as in Krasemann-Vermaseren}^{(1)} \text{ model)}$$

Because of the strong correlation between the helicity state and the ex-

perimental acceptance increasing contributions of the Helicity 0,1 states as the Q^2 of the virtual photons is increased will result in a systematically lower value for $\Gamma^{f_0}_{\gamma\gamma}$ than if Helicity 2 dominance is assumed at all Q^2 values. In the Krasemann Vermaseren model the evolution of the contributions of the helicity 0,1 states is predicted. The small value for $\Gamma^{f_0}_{\gamma\gamma}$ in the single tagged data may then be taken as evidence that the $\lambda=2$ contribution drops more rapidly with increasing Q^2 than the prediction of the model. However, the confidence level that $\Gamma^{f_0}_{\gamma\gamma}$ is the same for the tagged and the untagged data within the model is 15%, so a statistical fluctuation is still possible.

For a complete list of the TASSO results on radiative widths, including systematic errors, the reader is referred to the talk of Hilger.

Problems of Consistency of Interpretation of the f_0 Peak

5 different experiments presented data on the f_0, 4 of them TASSO, CELLO, JADE and MARK II on the $\pi^+\pi^-$ decay mode, and 1, the Crystal Ball, on $f_0\to\pi^0\pi^0$. All experiments found the mass to be below the standard value of 1273 MeV, but no consistent interpretation was given either of this shift or of the other possible structures near or under the f_0. To briefly summarise the results from the different experiments once more:

Crystal Ball
- $f_0\to\pi^0\pi^0$ Mass $\sim$ 30 MeV low, almost certainly not an instrumental shift
- No significant S*
- No background and so no interference effect
- No contribution from f'

CELLO
- $f_0\to\pi^+\pi^-$ Preliminary data, pions unidentified
- Mass $\sim$ 50 MeV low
- Hint of S*(980)

JADE
- $f_0\to\pi^+\pi^-$ Preliminary data, pions unidentified
- No f_0 mass or width quoted
- No evidence for S*(980) (see Fig. 31)

TASSO
- $f_0\to\pi^+\pi^-$ Pions unidentified
  Mass $\sim$ 30 MeV low in free fit (to f_0 only)
  Good fit to data book values including:
  - $S^*(980)\to\pi^+\pi^-$ (3 σ effect)
  - $f'\to K^+K^-$ improves fit, but of marginal statistical significance

MARK II
- $f_0\to\pi^+\pi^-$ Pions identified in a subsample of data
  Peak mass 30-40 MeV low
- No significant S*(980) signal
- Large continuum $\pi\pi$ background observed under the f_0
- f_0 continuum interference can explain mass shift and improves the fit to the data

More details are given on the results from MARK II in the talk of D. Burke. Here only the $\pi^+\pi^-$ mass spectrum is shown (Fig. 32). Introducing complete interference clearly improves the fit to the data and could explain the observed mass shift. Discounting the preliminary data from CELLO and JADE, the biggest differences of interpretation occur between the two most thoroughly analysed experiments MARK II and TASSO. As MARK II has a better acceptance at low masses and pion identification possibilities it seems likely that the 2π continuum is a real effect. If this were so the TASSO data should be re-interpreted, in particular the $S^*(980)$ peak would in this case become less significant, and the interference mechanism would avoid the necessity of introducing the $f'\to K^+K^-$ decay. Taking the MARK II results at their face value (mass shift produced by resonance continuum interference), the similar mass shift seen in the Crystal Ball data, where no such mechanism can operate still remains to be explained. As pointed out in discussion by Frazer it is expected that resonances will have different central values in different decay channels, but is a $\sim$ 40 MeV shift between $f_0\to\pi^+\pi^-$ and $f_0\to\pi^0\pi^0$ actually reasonable? Another difficulty is that a Born term with the same magnitude as that used by Burke is incompatible with the higher mass (>2 GeV/c^2) TASSO data. It would give a 20% contribution in the region where there is good absolute agreement between the data and the Q.E.D. ($ee\to ee\mu\mu$) contribution. The MARK II data presented here does not extend above masses of 1.7 GeV/c^2. The TASSO and MARK II data can be made compatible only by invoking a strong absorbtion of the Born term at high masses.

Finally it should be mentioned, as pointed out by Wacker, that there is a further free parameter the 'effective range' giving the strength of the barrier penetration factor in the Relativistic D wave. Breit-Wigner used to describe the mass distribution in the region of the f_0. Changing thus parameter from say 1 f to 2 f gives quite sizeable effects in the tails of the line shape and so may effect the quality of interference fits, but has little effect on the peak position.

All in all then it is clear that more work is needed before a consistent interpretation of the process:

$$ee \to Xee \quad \Big\lfloor \to \pi^+\pi^-,\ \pi^0\pi^0$$

in the mass region near the f_0 emerges. It seems clear that in any case $\Gamma^{f_0}_{\gamma\gamma} \sim$ 2-3 keV but much more detailed work (particularly involving particle identification) is needed before any finer conclusions can be drawn.

Wermes

Some of the most interesting preliminary results presented at this conference, in terms of their impact on physics as a whole, are the new quantitative indications that hard scattering processes do indeed occur in $\gamma\gamma$ collisions with about the theoretically expected[12],[13] cross section. The first indications of hard scattering processes were already presented at the Amiens meeting last year in the talks of Berger (PLUTO) and Hilger (TASSO). With the larger integrated luminosities now available quantitative comparisons have been made by both the JADE and TASSO groups. As the JADE results are fully covered in the talk of Cords I shall here concentrate on the TASSO results.

The TASSO results are based on singly tagged events and correspond to an integrated luminosity of 9320 nb^{-1}. The trigger required a tagged electron (energy >4 GeV in the forward detector) in coincidence with 1 or more charged tracks in the central detector with p_T >0.3 GeV. The following cuts were applied to isolate multihadron events resulting from $\gamma\gamma$

collisions:

- $\geq$ 4 charged tracks 1 with $p_T > 0.3$ GeV/c
  3 with $p_T > 0.2$ GeV/c
- Vertex requirements
- Beam gas events removed by proton identification
- 4.6 GeV $< W^{vis}_{\gamma\gamma} < 0.4 \times (2E_{Beam})$ where $W^{vis}_{\gamma\gamma}$ is the effective mass of the visible tracks, including also neutral energy in 52% of the solid angle.

In addition candidate 2-jet events were sought by maximising for each event the quality 'twoplicity' = T_2 defined by the relation:

$$T_2 = \underset{c_1,\, c_2}{\text{Max}} \; \frac{\left| \sum_{i \in c_1} \vec{p}_i \right| + \left| \sum_{i \in c_2} \vec{p}_i \right|}{\sum_{\text{all } i} |\vec{p}_i|}$$

The particles in a given event are assigned to the two classes c_1, c_2 chosen so that the expression within the curly brackets is maximised, and the particles so grouped are identified as coming from two 'jets'. The thrust or sphericity axis for the particles in each 'jet' can then be found in the normal way. Requiring also that:

- each 'jet' has $\geq$ 2 particles
- at least one 'jet' has $p^{(JET)} = \left| \sum \vec{p}_i \right| > 2$ GeV/c

60 events are found. In some cases the 'two jet' structure can be seen by eye. An example is given in Fig. 33. Before proceeding to examine 'jet' quantities obtained as described above it is of interest to look at the inclusive p_T distribution of the hadrons in the events to see if there is evidence already for the p_T^{-4} behaviour expected from the leading hard scattering process. Fig. 34 shows $d\sigma/dp_T^2$ for the new TASSO multiprong data. At low p_T the data fits well to a e^{-6p_T} dependance. To compare the $\gamma\gamma$ induced data with the 'conventional' high p_T tail of the normal diffractive process, due mainly to 'constituent interchange' or 'higher twist' contributions where single mesons, rather than quarks, are scattered to high p_T in the subprocess, ISR data for inclusive π^+ production in pp collisions at $\sqrt{s}$ = 45 GeV and 90° in the CM system are shown. The high p_T tail of the ISR data, which also fits well to e^{-6p_T} below p_T of $\sim$ 1 GeV falls slightly more slowly than the p_T^{-6} behaviour

expected from constituent interchange or 'higher twist' diagrams. In contrast the $\gamma\gamma$ data seems already consistent with 'dimensional scaling' p_T^{-4} behaviour for $p_T \cdot 2$ GeV/c.

To make a quantitative comparison with the cross section expected from the lowest order hard scattering graph (Fig. 35) an estimate was made of the background from other processes in the 60 candidate events. The following contributions were estimated:

- Beam gas scattering	5%
- $l\gamma$ annihilation with initial state radiation	6%
- $l\gamma$ τ production	0.5%
- VDM like hadron production	0.4%
- 2γ τ production	3%

In total these give $\sim$ 15% background leaving signal of 51 2-jet events.

These events were compared with a Monte Carlo simulation of the process in Fig. 35. The quark distributions were generated using the Vermaseren QED program with cross section $\propto 3\ e_q^4$ and m_q = 0.3 GeV/c^2 for u, d, s, and 1.5 GeV/c^2 for c. The quark fragmentation was done using either the standard Feynman-Field prescription including vector mesons, or a simple all pion model where pions are generated according to phase space, but with limited p_T relative to the jet axis. Putting in the cuts and the experimental luminosity 33 events are expected from the lowest order graph. Fig. 36 shows the comparison of the background subtracted data with the Monte Carlo for the distribution dN/dp_T^2(jet). It can be seen that a discrepancy occurs predominantly at low values of p_T^2(jet). Such a discrepancy is not surprising since it is in this region that higher twist contributions and hard scattering processes involving gluon radiation (see the talks of Kajantie and Davier at this conference) are expected to be important. Under the assumption that the process in Fig. 35 completely describes the data the cross section of the high p_T events is most conveniently expressed in terms of:

$$R_{\gamma\gamma} = \frac{\sigma_{\gamma\gamma \to q\bar{q}}}{\sigma_{\gamma\gamma \to \mu\mu}} = 3 \sum e_{q_i}^4 = 1.26 \qquad \text{for u, d, s, c quarks}$$

In Fig. 37 is shown the experimental value of $R_{\gamma\gamma}$ given by the above assumption, using standard fragmentation parameters, which have not however been fitted in an optimal way to the data. A more detailed investigation of the dependance of $R_{\gamma\gamma}$ on these parameters is in progress. In view of this, Fig. 37 should be taken only as an indication of the trend of the data with increasing p_T.

To summarise one can say that within the rather limited statistics of the data there is agreement between experiment and the expectations from the 'QED graph' of Fig. 35 for p_T^{MIN}(jet) $\cdot$ 3 GeV/c in particular the dimensional scaling behaviour $\propto p_T^{-4}$ is already evident even at these rather low transverse momenta - a situation very different to that found in hadron-hadron collisions. As the graph in Fig. 35 involves only photons and quarks it is perhaps a little premature to say there is direct evidence for the validity of Q.C.D. in $\gamma\gamma$ collisions, that the data are described by this simple graph at sufficiently high p_T is a consequence of the quark parton model, so it is really, as pointed out by Brodsky, the asymptotically free nature of Q.C.D. which is being tested. QCD tests in the strict sense, where the existence of gluons is required await the observation of higher order processes. Already, however, the good agreement between $R_{\gamma\gamma}^{exp}$ and $R_{\gamma\gamma}^{thy}$, confirms the existence of coloured fractionally charged quarks. It is perhaps the clearest experimental evidence against the Han-Nambu[14] integrally charged quark model in which[15] $R_{\gamma\gamma}$ = 10/3 below colour threshold (see Fig. 37).

Acknowledgements

I should like to thank all of the speakers in the discussion session for giving so freely of their time during the preparation of the written version of this talk, and also the Organising Secretary of the Conference; George London for the constant encouragement which ensured the work was completed within a reasonably short time after the date of the meeting.

DISCUSSION

C - Hilger

TASSO has of course tried to explain the funny shape of the observed $\pi^+\pi^-$ resonance by an interference with the Born term continuum. We find it impossible to allow enough $\pi^+\pi^-$ continuum for a visible interference effect. When we try a fit allowing for QED lepton-pair production and f resonance we obtain:

$$\frac{N\ Data}{N\ QED} = 0.94 \pm 0.04 \pm 0.08$$

We have also studied the variation of the QED subtracted data as a function of the cut on the total transverse momentum P_T of the pair. We find the mass spectrum unchanged until a P_T cut of more than about 0.4 GeV/c. The inclusive pairs creep into the sample and the mass distribution below the f peak becomes structureless in the S^* region.

C - Burke

I would like to comment on the f (1270) line shape. The issue here is whether or not there is an S^* (980) which accounts for $\sim$ 20% of the events in the peak. It is important to properly look at the complete $\pi\pi$ spectrum below the f. In particular, since our measurements show that the $\pi\pi$ rises fairly sharply below the f, then forcing the spectrum to zero at masses $\sim$ 800 MeV can artificially produce a peak in the remaining spectrum.

C - Renard

If the $\rho\rho$ enhancement is due to a resonance, the $\omega\omega$ channel can also resonate as soon as the mass of the resonance is above the $\omega\omega$ threshold; the opening of the $\omega\omega$ channel is much sharper than the $\rho\rho$ one (because of the small ω width); the coupling constant of the resonance to $\omega\omega$ can be comparable to that of $\rho\rho$. They are also several other allowed channels for the decay of this resonance (ex: $\eta\pi\pi$,....).

TABLE 1

Predictions of different models for $ee \to eeV^+V^-$ cross sections relative to $ee \to ee\rho^0\rho^0$

Channel	$\rho^0\rho^0$	$\rho^+\rho^-$	$\omega\omega$	$\rho^0\omega$
Model				
VDM	1	0	1/81	1/9
Quark model (Krammer)	1	2	1	36/25
Quark model (Biswal and Misra)	1	4/25	allowed	allowed
Resonance	1	2	allowed	0

References

1) H. Krasemann and J.A.M. Vermaseren
CERN TH-2918 August 1980

2) J.H. Field
Nuclear Phys B168 (1980),477

3) A. Courau
Orsay Report LAL/81-03 February 1981

4) J. Layssac and F.M. Renard, Montpellier
pre-print PM/80/11

5) H. Goldberg and T. Weiler, Boston
pre-print Boston NUB 2488, 1981

6) M. Krammer
private communication

7) K. Biswal and S.P. Misra, Bhudaneswar (India)
pre-print IP/BBSR/80-18, October 1980

8) S.J. Brodsky, T. Kinoshita and H. Terezawa
Phys. Rev. D4 (1971), 1532

9) P. Jenni
Proceedings of the International Workshop on $\gamma\gamma$ Collisions
Amiens/France, April 1980. Published by Springer Verlag, p. 47

10) N. Barash-Schmidt et al.
Reviews of Modern Physics, Vol. 52 No. 2, April 1980

11) J. Babcock and J.L. Rosner
Phys. Rev. D14 (1976), 1286

12) S.J. Brodsky, T.A. de Grand, J.F. Gunion and J. Weis
Phys. Rev. Lett. 41 (1978), 672

13) K. Kajantie
Physica Scripta 19 (1979), 230

14) M.Y. Han and Y. Nambu
Phys. Rev. 139 (1965), 1006

15) see for example P. Landshoff in:
Proceedings of the LEP Summer Study (Les Houches 1978)
CERN 79-01, p. 555.

Figures

Fig. 1: Effect of different sampling intervals on Monte Carlo generation efficiency.
a) Uniform intervals, $\varepsilon \approx 50\%$,
b) Optimised intervals, $\varepsilon \approx 100\%$.

Fig. 2: Comparison of Monte Carlo generated events (points with error bars) with distributions calculated using Vermaseren's integration program (solid histogram).
a) $ee \to \mu\mu ee$, μ^+ lab angle;
b) $ee \to \mu\mu ee$, opening angle between μ^+ and μ^-.

Fig. 3: Comparison of luminosity functions given in Ref(2) (solid curves) with results of Kawabata's Monte Carlo integrator (solid points)

Fig. 4: Distribution of the square of the total transverse momentum for 4 prong events

Fig. 5: $\Sigma p_y^{\,i}$ versus $\Sigma p_x^{\,i}$ (orthogonal components of the total transverse momentum) for 4 prong events. 1.2 GeV < M(4 prong) < 6.0 GeV.

Fig. 6: Scatter plot of unequal sign dipion combinations (two entries per event) for 4 prong events with 1.4 GeV < M(4 prong) < 1.7 GeV

Fig. 7: Scatter plot of equal sign dipion combinations (one entry per event) for 4 prong events. Cuts as in Fig. 6

Fig. 8: Distributions of the average mass of dipion combinations in 4 prong events. Cuts as in Fig. 6. Solid histogram: like sign combinations, dotted histogram: unlike sign combinations.
a) Data,
b) Monte Carlo with a non symmetrised matrix element,
c) Monte Carlo with a symmetrised matrix element.

Fig. 9: Distributions of the $\pi^+\pi^-$ and $\pi^+\pi^-\gamma$ invariant mass for 2 prong and 1γ events (no particle identification).

Fig. 10: π-e separation given by simultaneous measurement of dE/dx (ordinate) and p (abscissa)

Fig. 11: $\pi^+\pi^-$ mass spectrum for 2 prong and 1γ events after removing identified electrons

Fig. 12: $\pi^+\pi^-\gamma$ mass spectrum for 2 prong and 1γ events after removing identified electrons. Shaded histogram: Events with $\pi^+\pi^-$ in the ρ^0 region $600 < M(\pi^+\pi^-) < 900$ MeV

Fig. 13: Geometrical construction of the Crystal Ball

Fig. 14: A 4γ event as observed in the NaI counters of the Crystal Ball

Fig. 15: $M_{\gamma\gamma}$(high) versus $M_{\gamma\gamma}$(low) 4γ events with $1.04 < M(4\gamma) < 1.5$ GeV/c^2 and $(p_T^{4\gamma})^2 < 0.03$ (GeV/c)^2

Fig. 16: Background subtracted $\pi^0\pi^0$ mass distribution

Fig. 17: Background subtracted $\pi^0\pi^0$ mass distribution. Data with low trigger threshold

Fig. 18: Monte Carlo background subtracted $\pi^0\pi^0$ mass distribution

Fig. 19: $\gamma\gamma$ Effective mass distribution. Cuts as in Fig. 15

Fig. 20: Angular distribution of π^0 relative to the beam direction in the f_0 rest frame. The fitted contributions of helicity 2, 1, 0 states are indicated

Fig. 21: $M_{\gamma\gamma}$ (high) versus $M_{\gamma\gamma}$ (low) 4γ events with cuts as in Fig. 15 and $\pi^0\pi^0$ combinations removed

Fig. 22: Background subtracted $\pi^0\eta$ mass spectrum. Cuts as in Fig. 21

Fig. 23: 2 prong $\pi\pi$ mass distribution. Points with error bars: data. Solid, dashed and dotted histograms $ee\to\mu\mu$ Monte Carlo normalised in different regions as described on the figure.

Fig. 24: $|\Sigma\vec{p}_T|$ versus $\pi\pi$ mass for 2 prongs

Fig. 25: Subtracted $\pi\pi$ mass spectrum for 2 prong events (CELLO)

Fig. 26: $\pi\pi$ mass spectrum for untagged 2 prong events (TASSO)

Fig. 27: Subtracted $\pi\pi$ mass spectrum for untagged 2 prong events (TASSO). Fits to f_0 and S^* using data book masses and widths are shown

Fig. 28: As Fig. 27 except fit contributions due to f_0, S^* and f' ($f'\to K^+K^-$) are shown

Fig. 29: Subtracted centre of mass decay distribution for the f_0 region: $1.1 < M_{\pi^+\pi^-} < 1.4$ GeV/c^2 (TASSO). The curves indicate the distributions expected for pure $\lambda = 0, 1, 2$ helicity states.

Fig. 30: $\pi\pi$ mass spectra for singly tagged 2 prong events (TASSO). Main distribution: unsubtracted, Inset: subtracted.

Fig. 31: Preliminary $\pi\pi$ mass spectrum for untagged 2 prong events (JADE)

Fig. 32: $\pi\pi$ mass spectrum for untagged 2 prong events (MARK II). The effect of a $\pi\pi$ Born term interfering with the f_0 is shown

Fig. 33: A candidate event for the process $ee\to ee+2$ jets with single tag

Fig. 34: $d\sigma/dp_T^2$ for $\gamma\gamma \to$ multihadron events (single tag) in comparison with ISR data (open circles)

Fig. 35: Lowest order diagram giving 2 high p_T quark jets

Fig. 36: p_T^2 distribution for 'jets' in single tag multihadron events. See text for the kinematic definition of a jet.

Fig. 37: Dependance of $R_{\gamma\gamma}$ on p_T^{MIN}(jet)

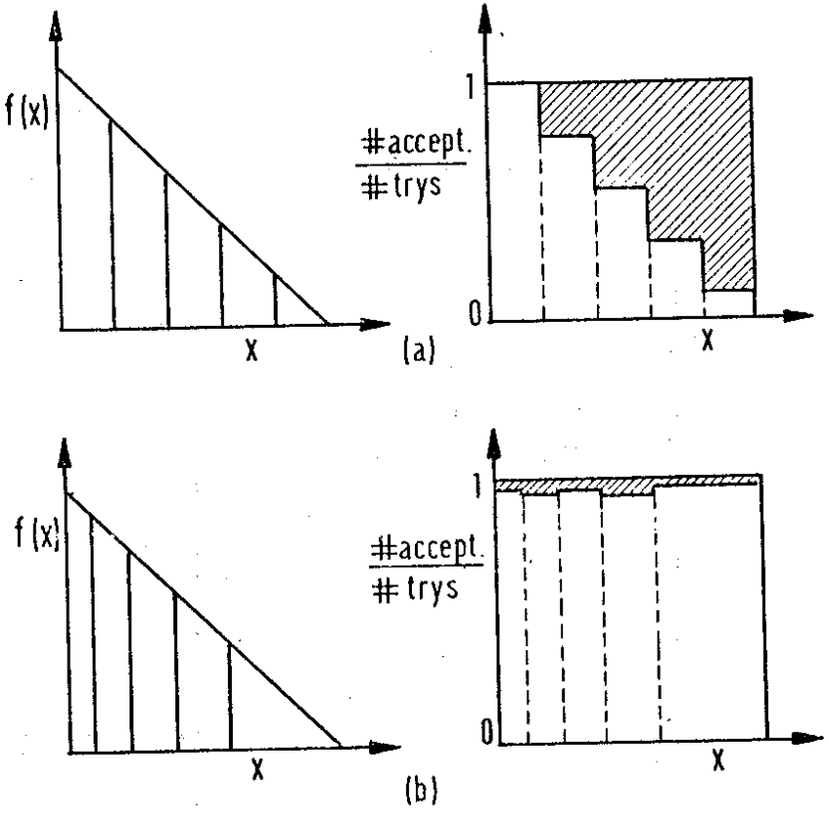

Fig. 1: Effect of different sampling intervals on Monte Carlo generation efficiency.
a) Uniform intervals, $\varepsilon \sim 50\%$,
b) Optimised intervals, $\varepsilon \sim 100\%$.

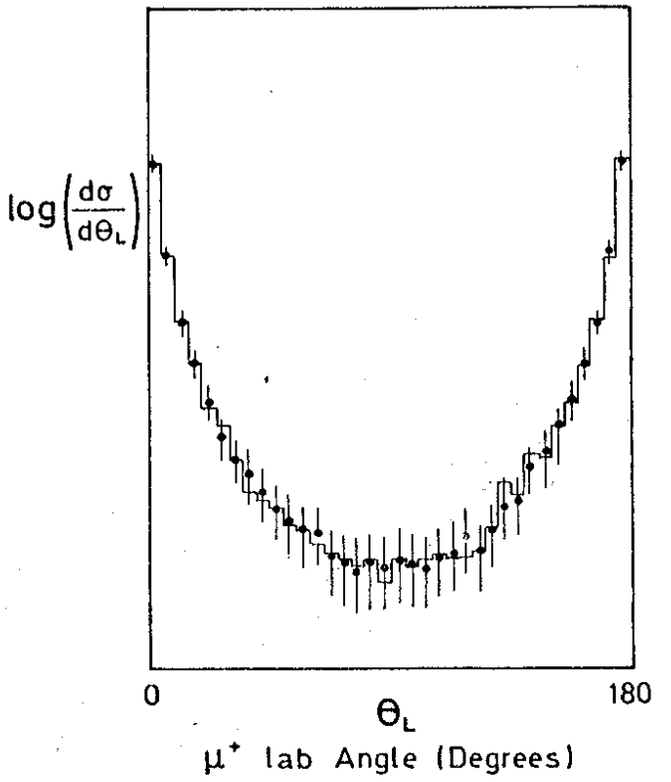

Fig. 2: Comparison of Monte Carlo generated events (points with error bars) with distributions calculated using Vermaseren's integration program (solid histogram).
a) $ee \to \mu\mu ee$. μ^+ lab angle;

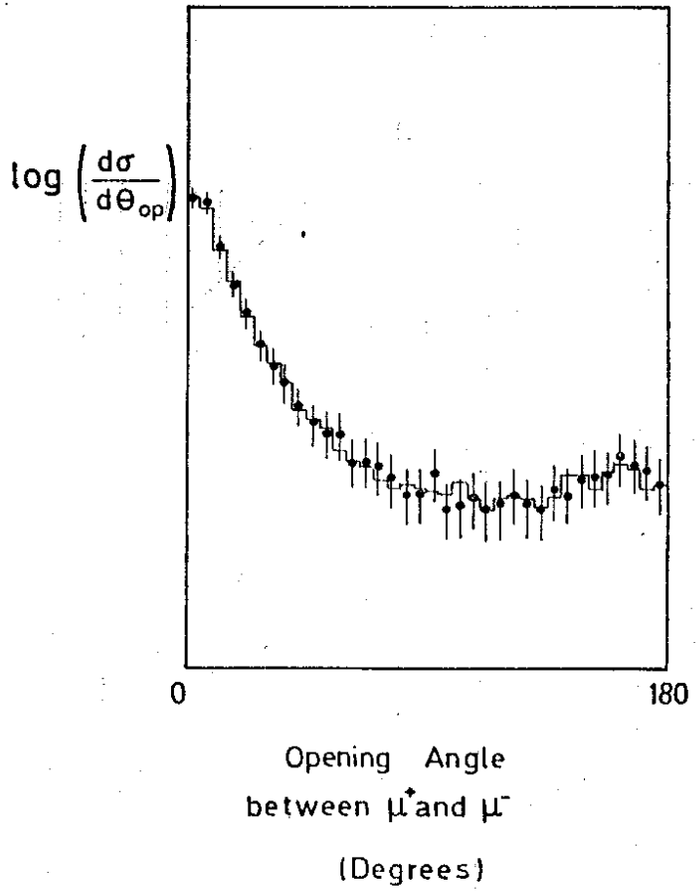

Fig. 2: Comparison of Monte Carlo generated events (points with error bars) with distributions calculated using Vermaseren's integration program (solid histogram)
b) ee → μμee, opening angle between μ^+ and μ^-.

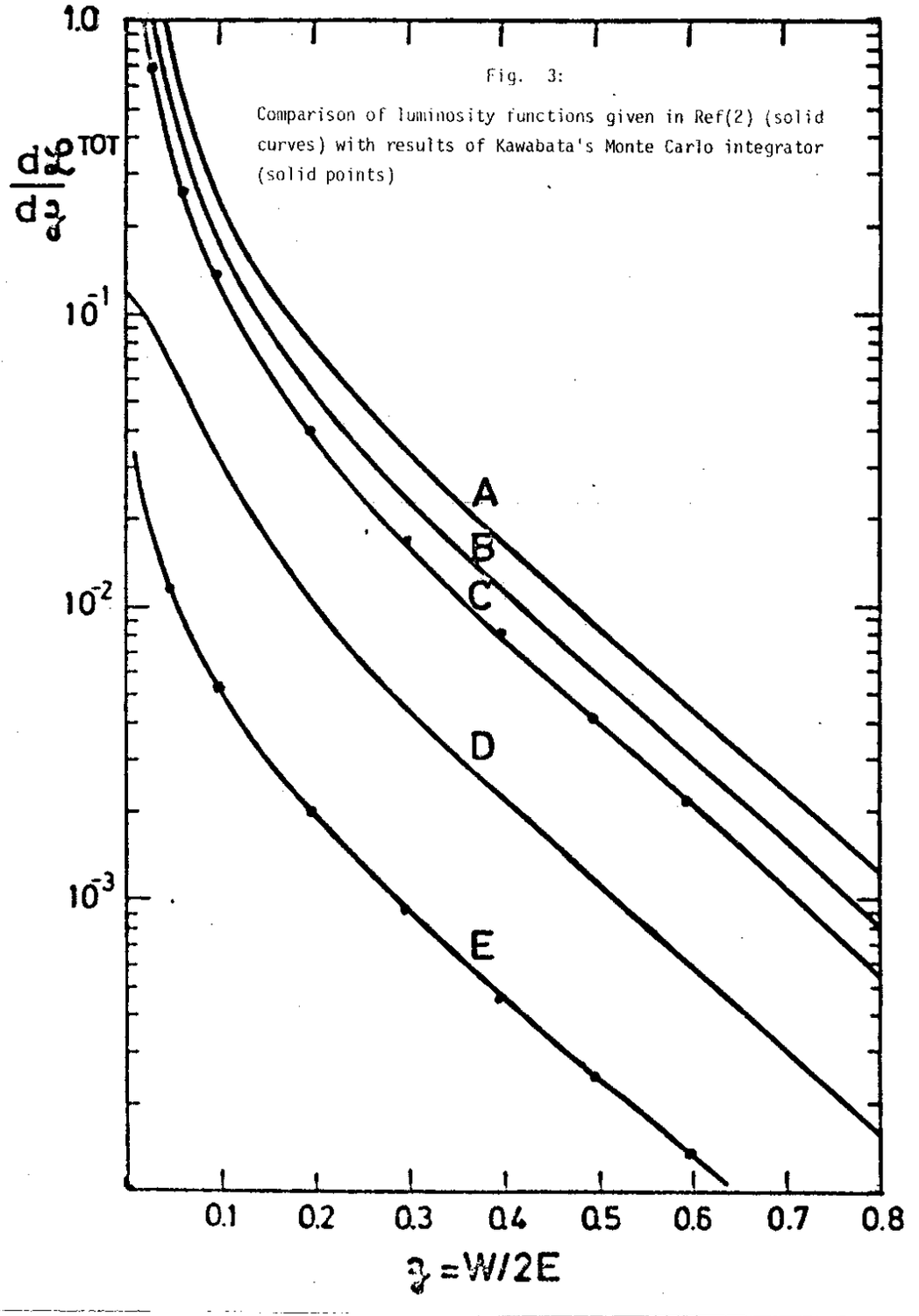

Fig. 3:
Comparison of luminosity functions given in Ref(2) (solid curves) with results of Kawabata's Monte Carlo integrator (solid points)

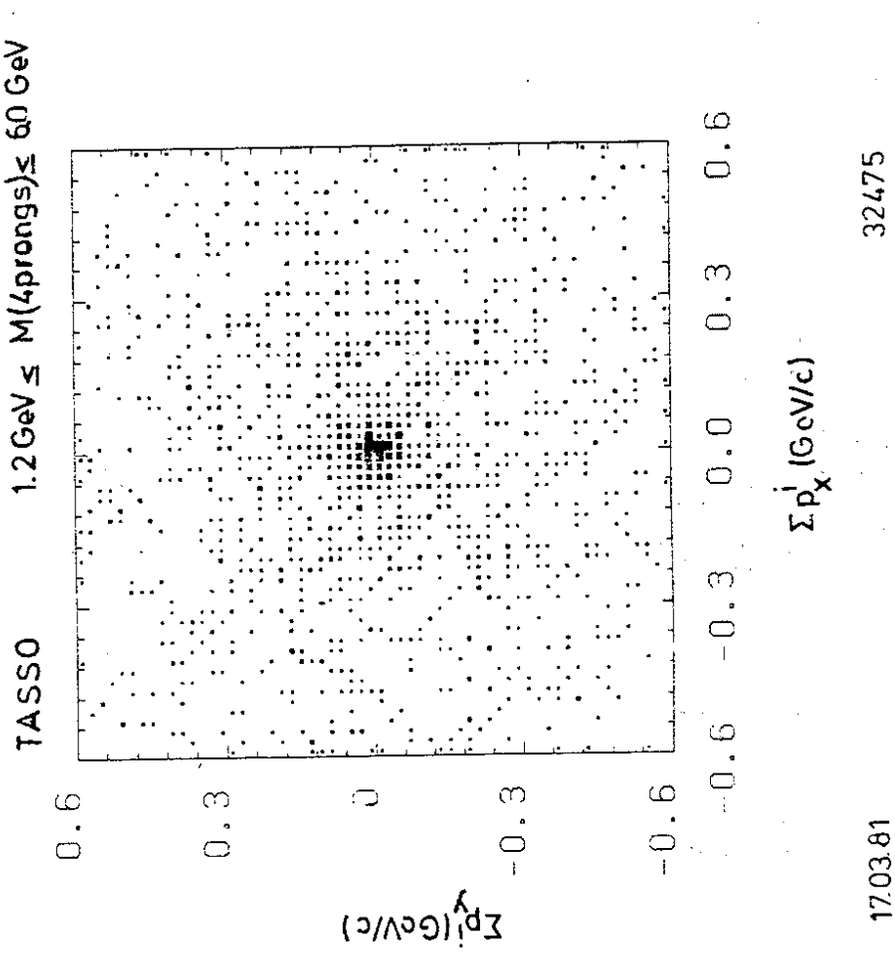

Fig. 5: Σp_y^i versus Σp_x^i (orthogonal components of the total transverse momentum) for 4 prong events. 1.2 GeV < M(4 prong) < 6.0 GeV.

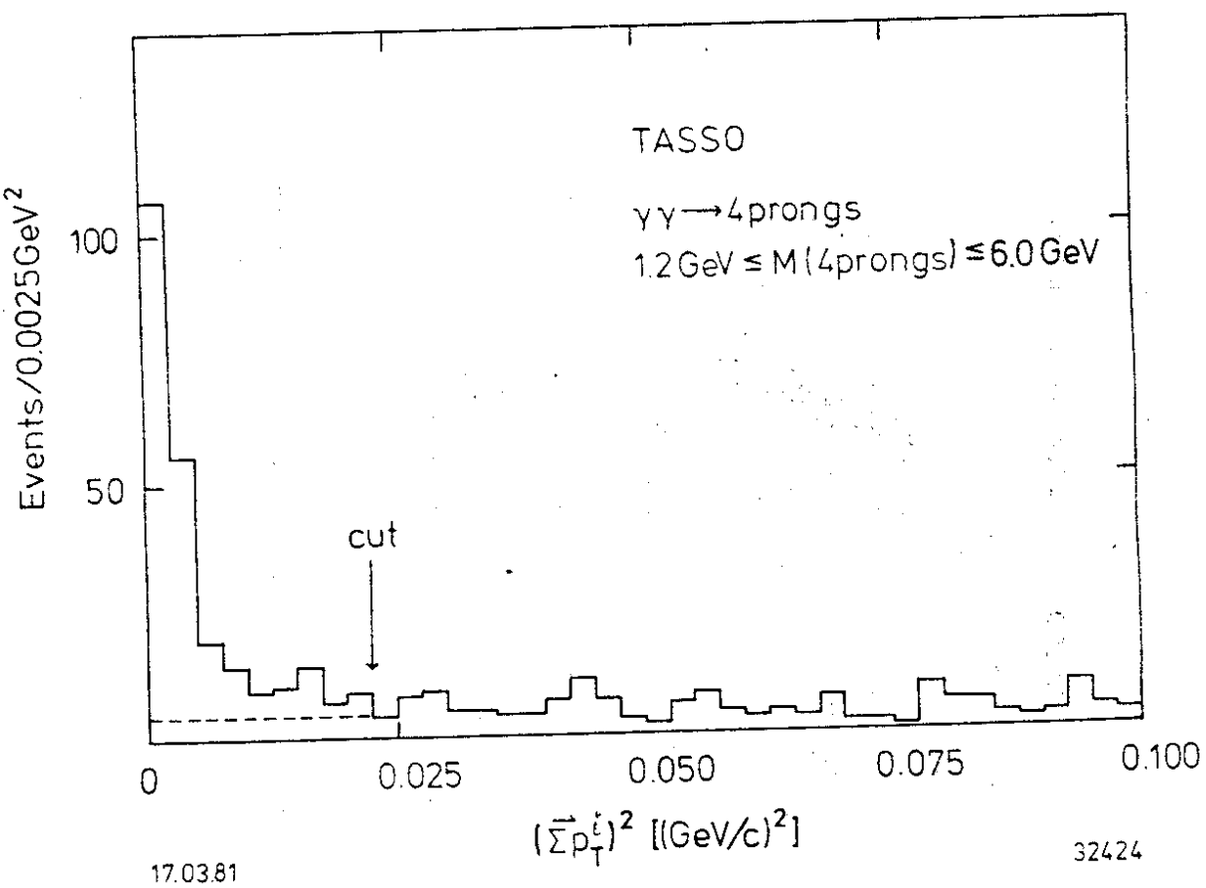

Fig. 4: Distribution of the square of the total transverse momentum for 4 prong events

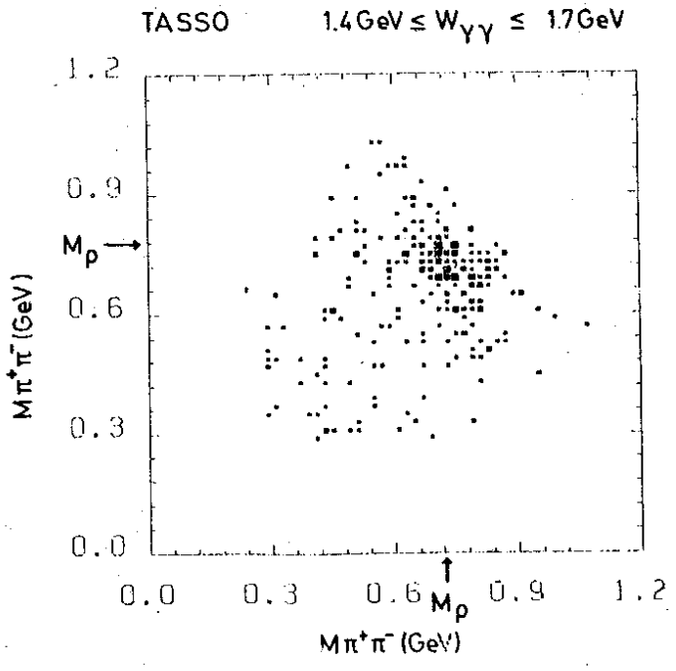

Fig. 6: Scatter plot of unequal sign dipion combinations (two entries per event) for 4 prong events with 1.4 GeV < M(4 prong) < 1.7 GeV

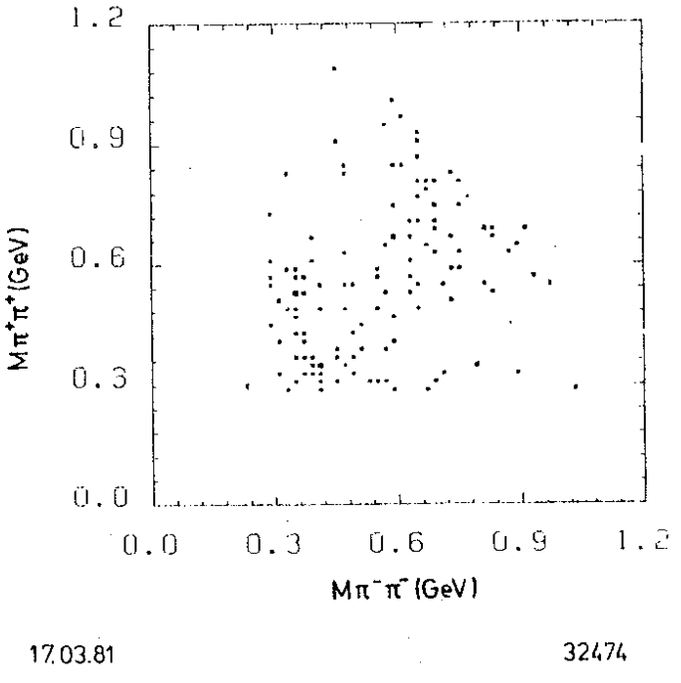

Fig. 7: Scatter plot of equal sign dipion combinations (one entry per event) for 4 prong events. Cuts as in Fig. 6

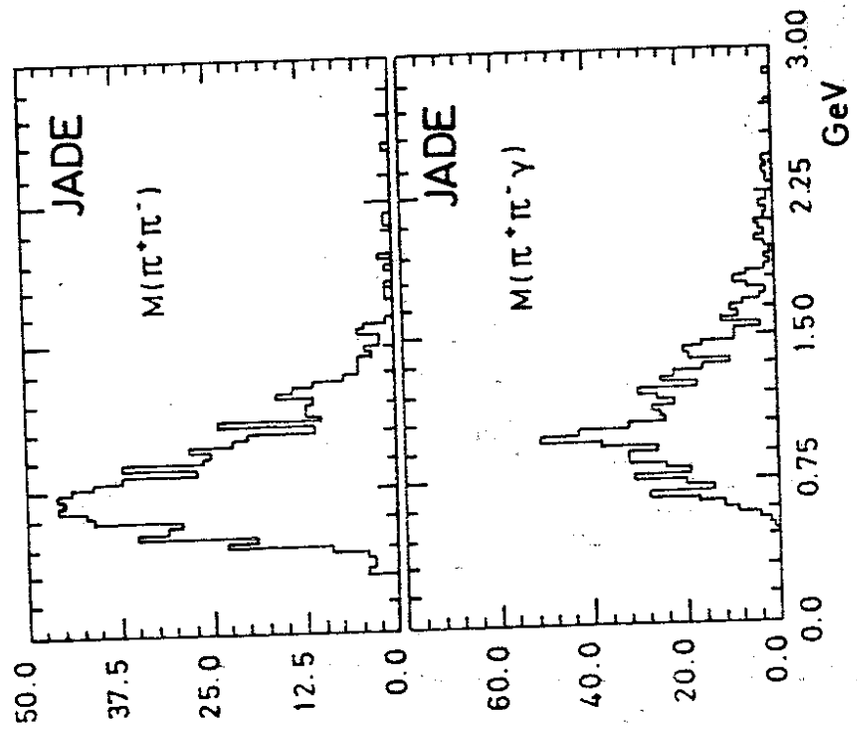

Fig. 9: Distributions of the $\pi^+\pi^-$ and $\pi^+\pi^-\gamma$ invariant mass for 2 prong and 1γ events (no particle identification)

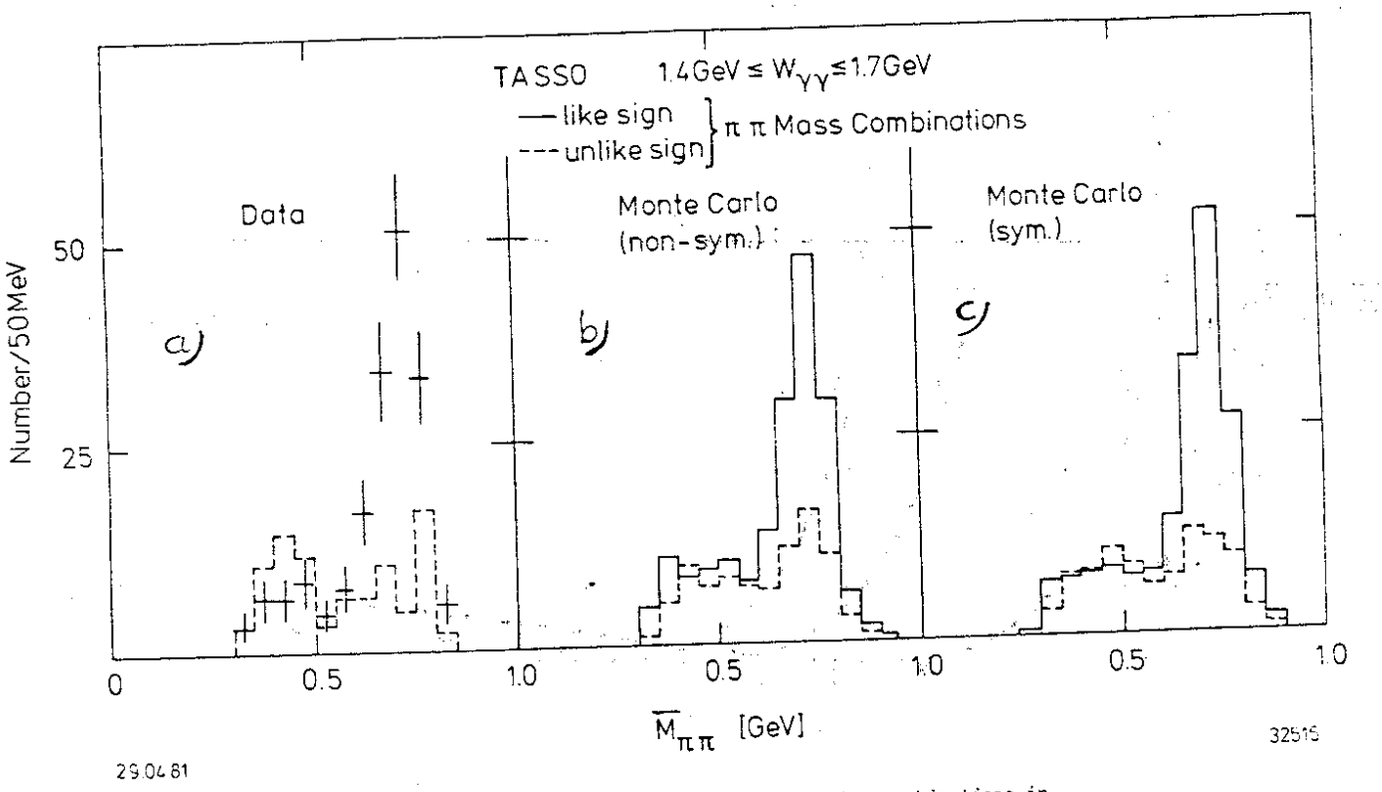

Fig. 8: Distributions of the average mass of dipion combinations in 4 prong events. Cuts as in Fig. 6. Solid histogram: like sign combinations, dotted histogram: unlike sign combinations.

a) Data,

b) Monte Carlo with a non symmetrised matrix element,

c) Monte Carlo with a symmetrised matrix element.

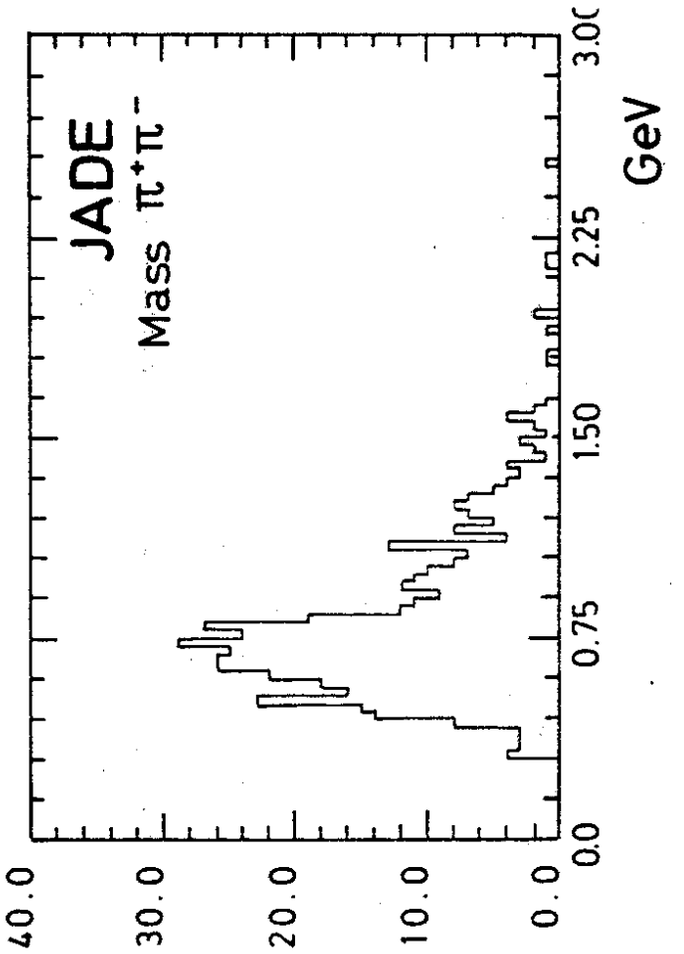

Fig. 11: $\pi^+\pi^-$ mass spectrum for 2 prong and 1γ events after removing identified electrons

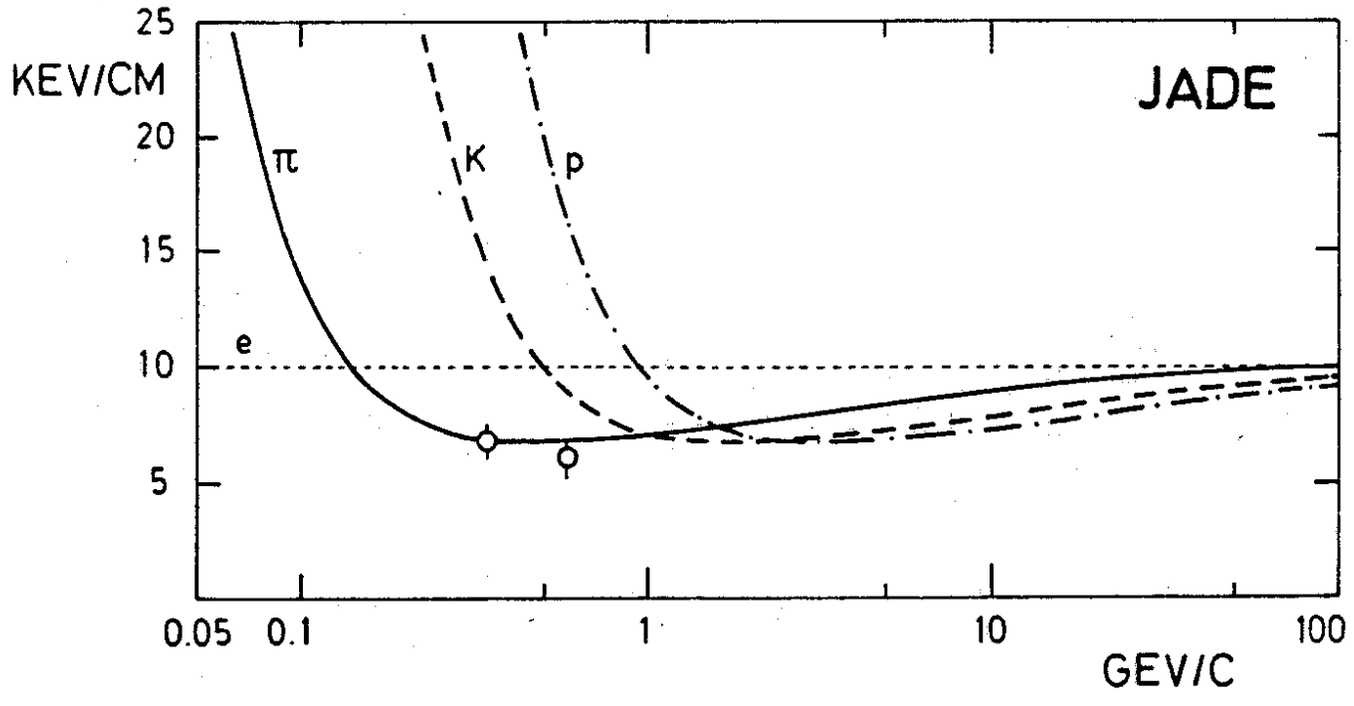

Fig. 10: π-e separation given by simultanebus measurement of dE/dx (ordinate) and p (abscissa)

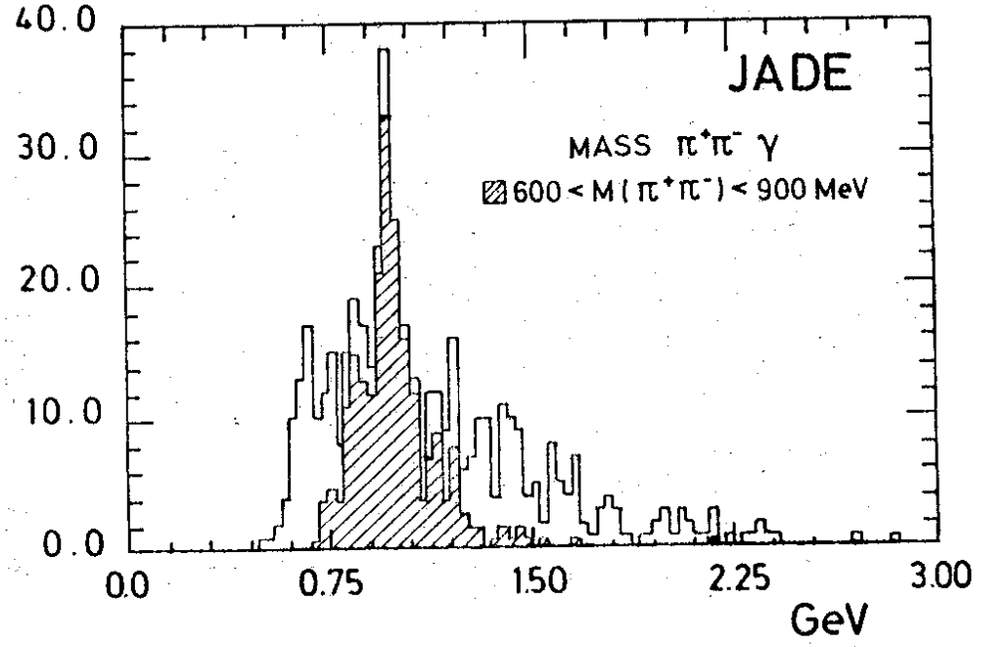

Fig. 12: $\pi^+\pi^-\gamma$ mass spectrum for 2 prong and 1γ events after removing identified electrons. Shaded histogram: Events with $\pi^+\pi^-$ in the ρ^0 region $600 < M(\pi^+\pi^-) < 900$ MeV

CRYSTAL BALL
GEOMETRY AND JARGON

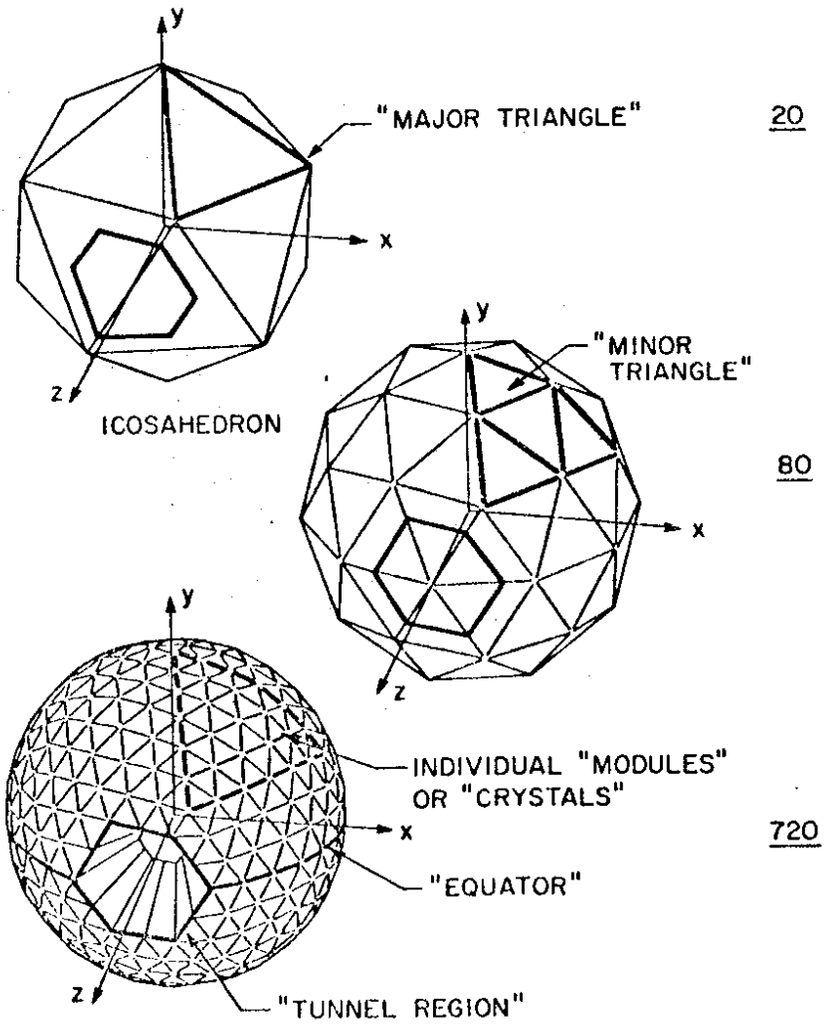

Fig. 13: Geometrical construction of the Crystal Ball

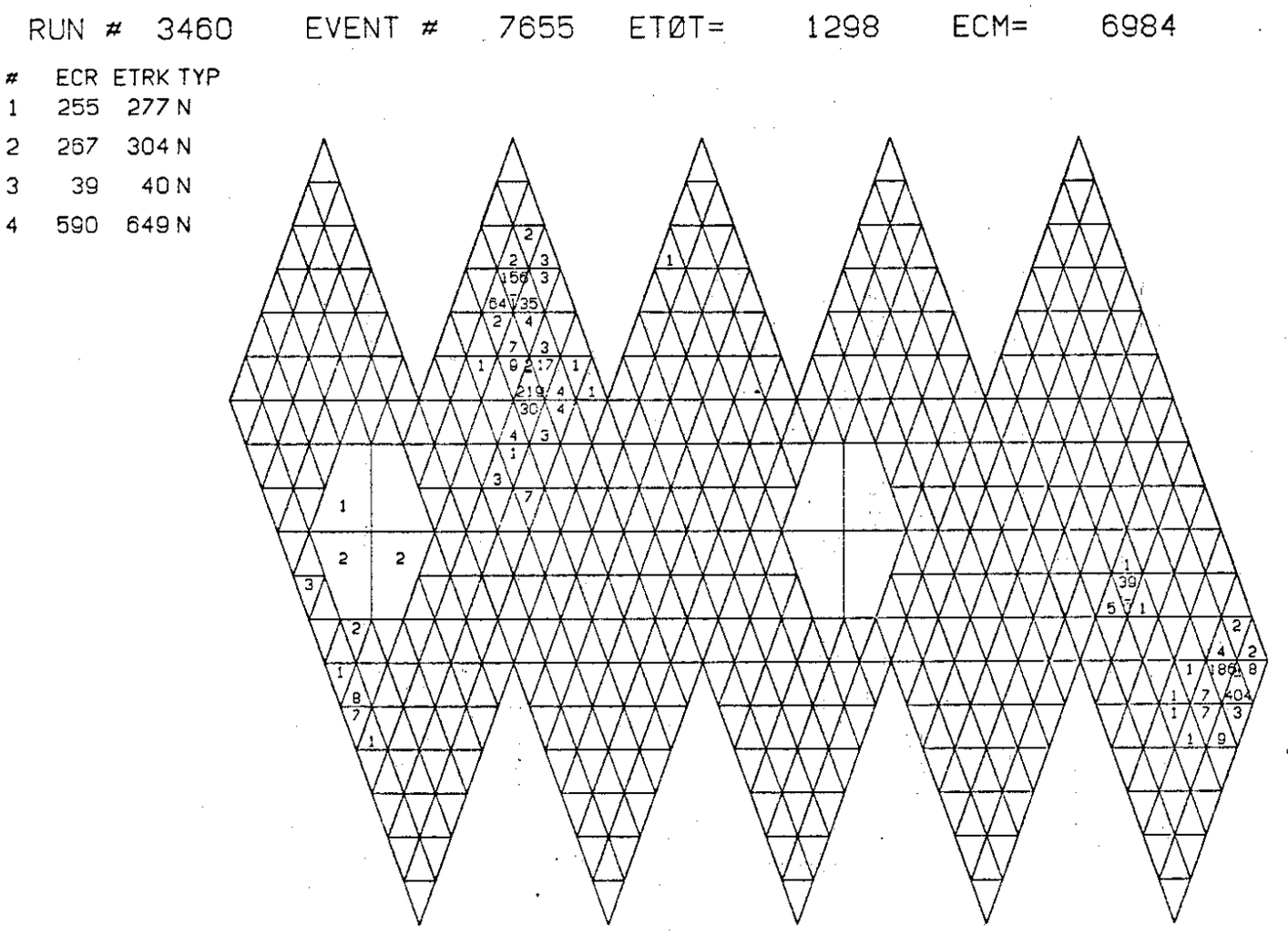

Fig. 14: A 4γ event as observed in the NaI counters of the Crystal Ball

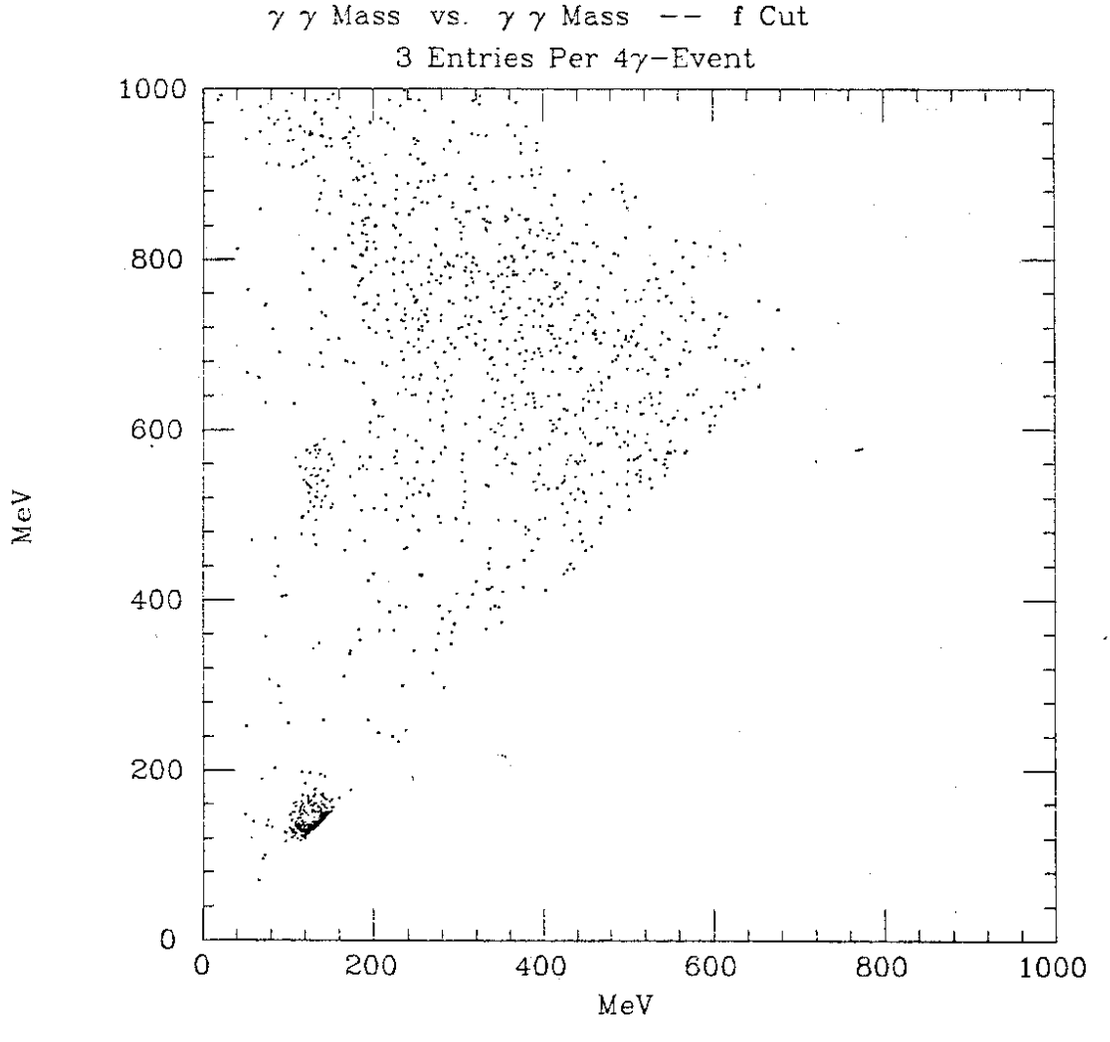

Fig. 15: $M_{\gamma\gamma}$(high) versus $M_{\gamma\gamma}$(low) 4γ events with $1.04 < M(4\gamma) < 1.5$ GeV/c^2 and $(p_T^{4\gamma})^2 < 0.03$ (GeV/c)^2

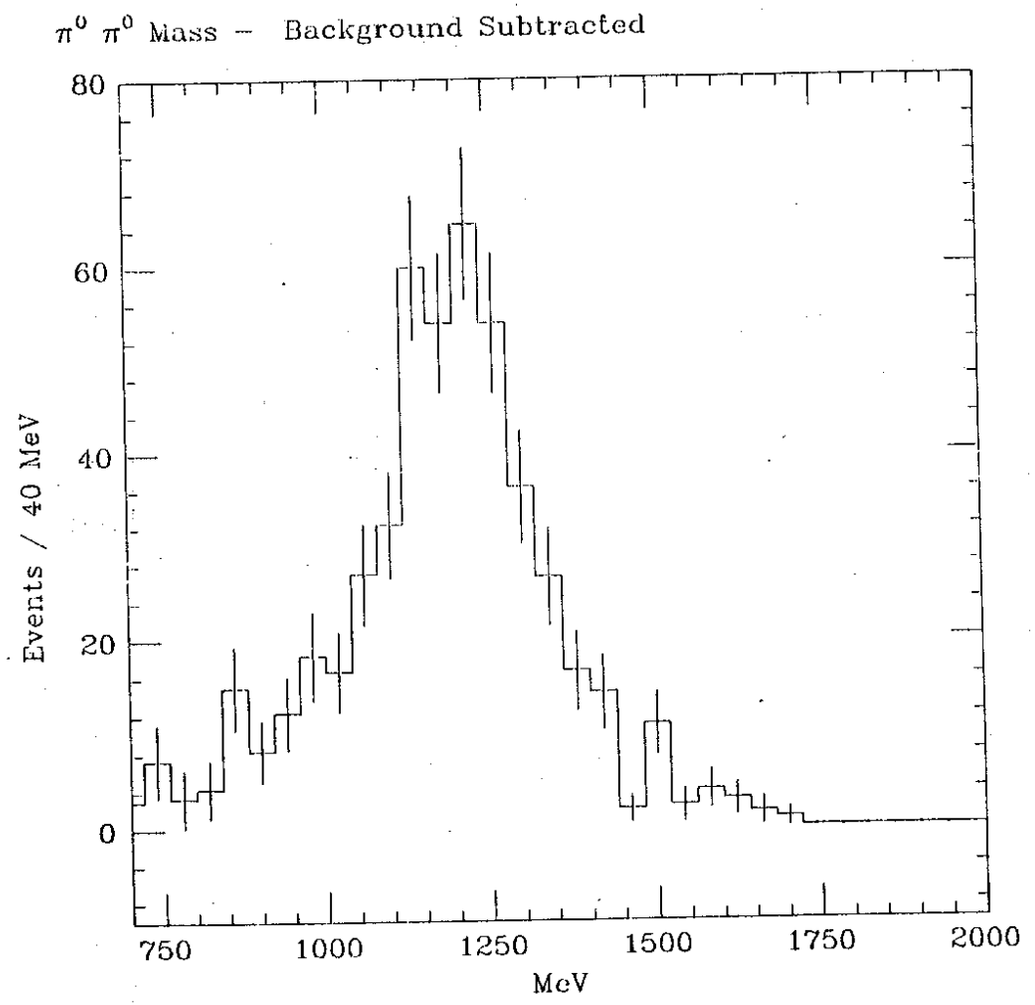

Fig. 16: Background subtracted $\pi^0\pi^0$ mass distribution

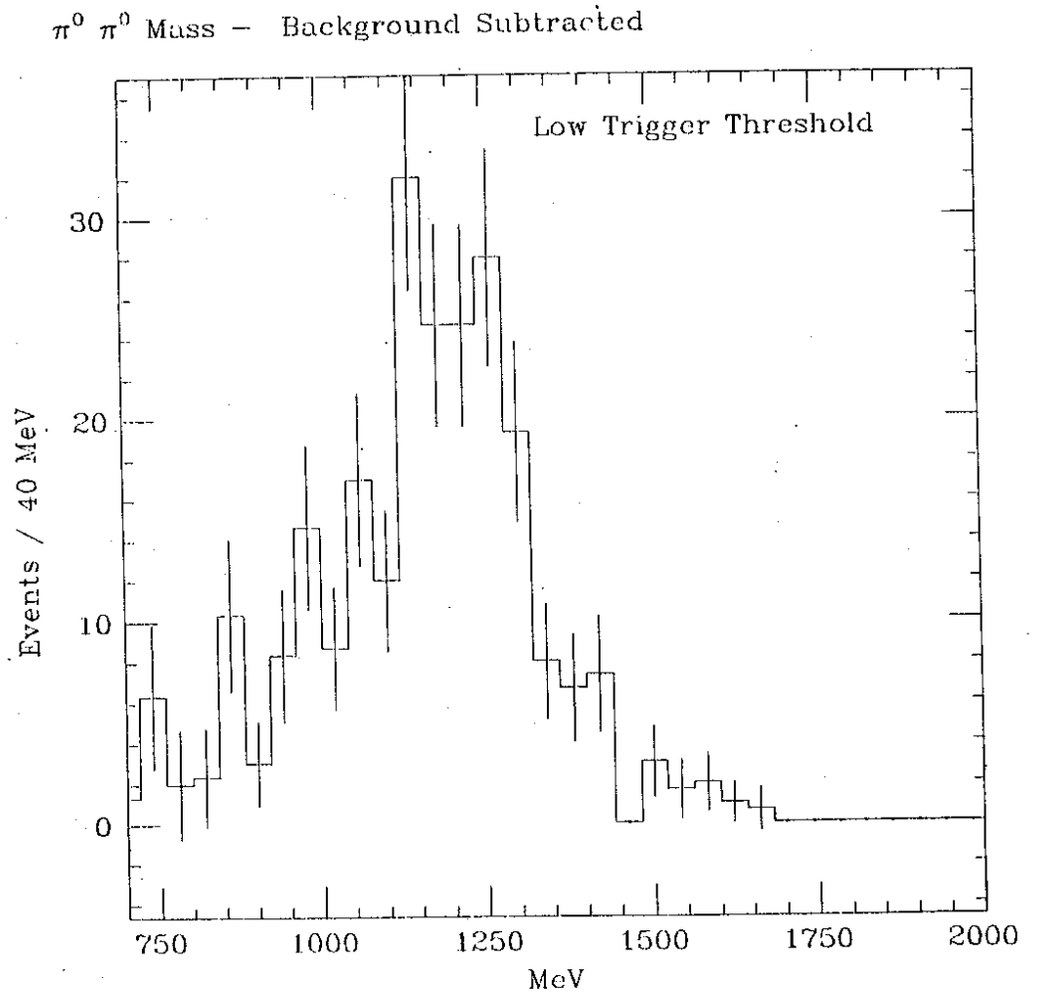

Fig. 17: Background subtracted $\pi^0\pi^0$ mass distribution. Data with low trigger threshold

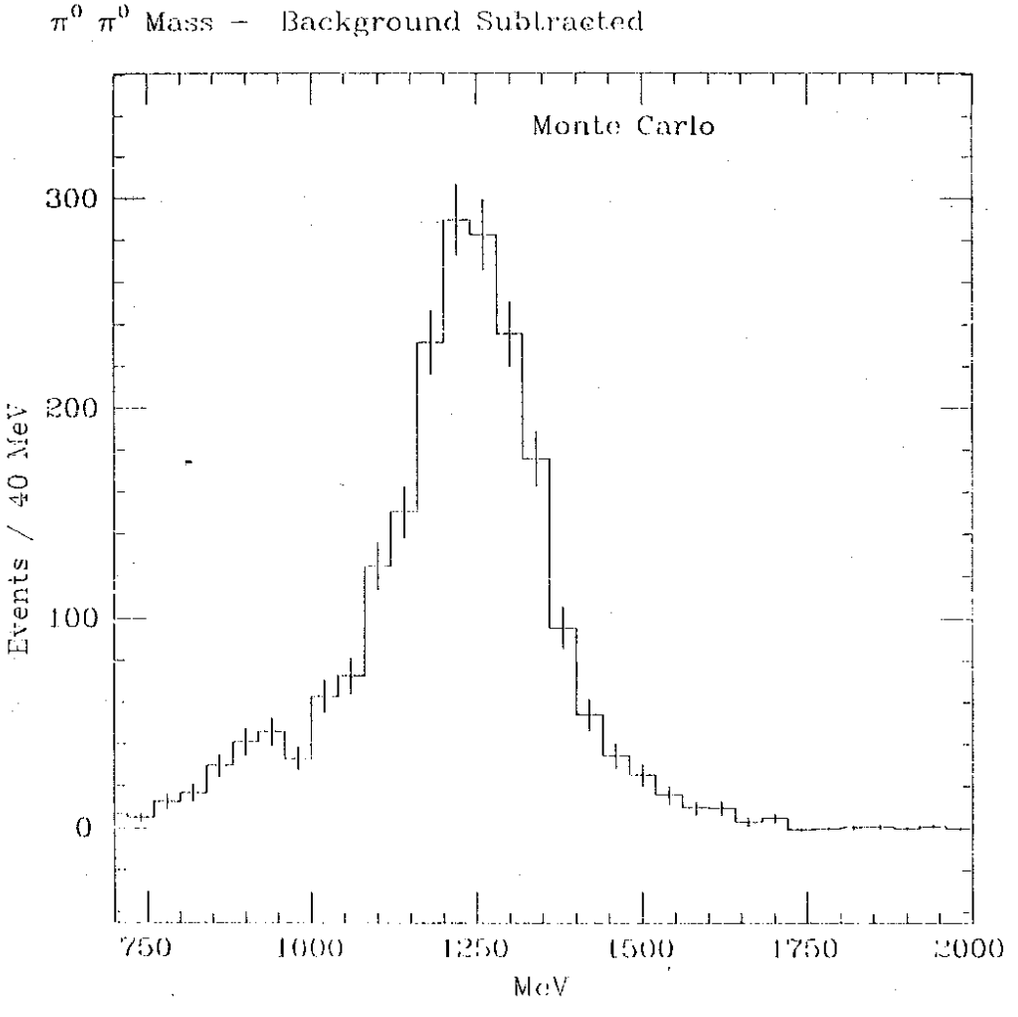

Fig. 18: Monte Carlo background subtracted $\pi^0\pi^0$ mass distribution

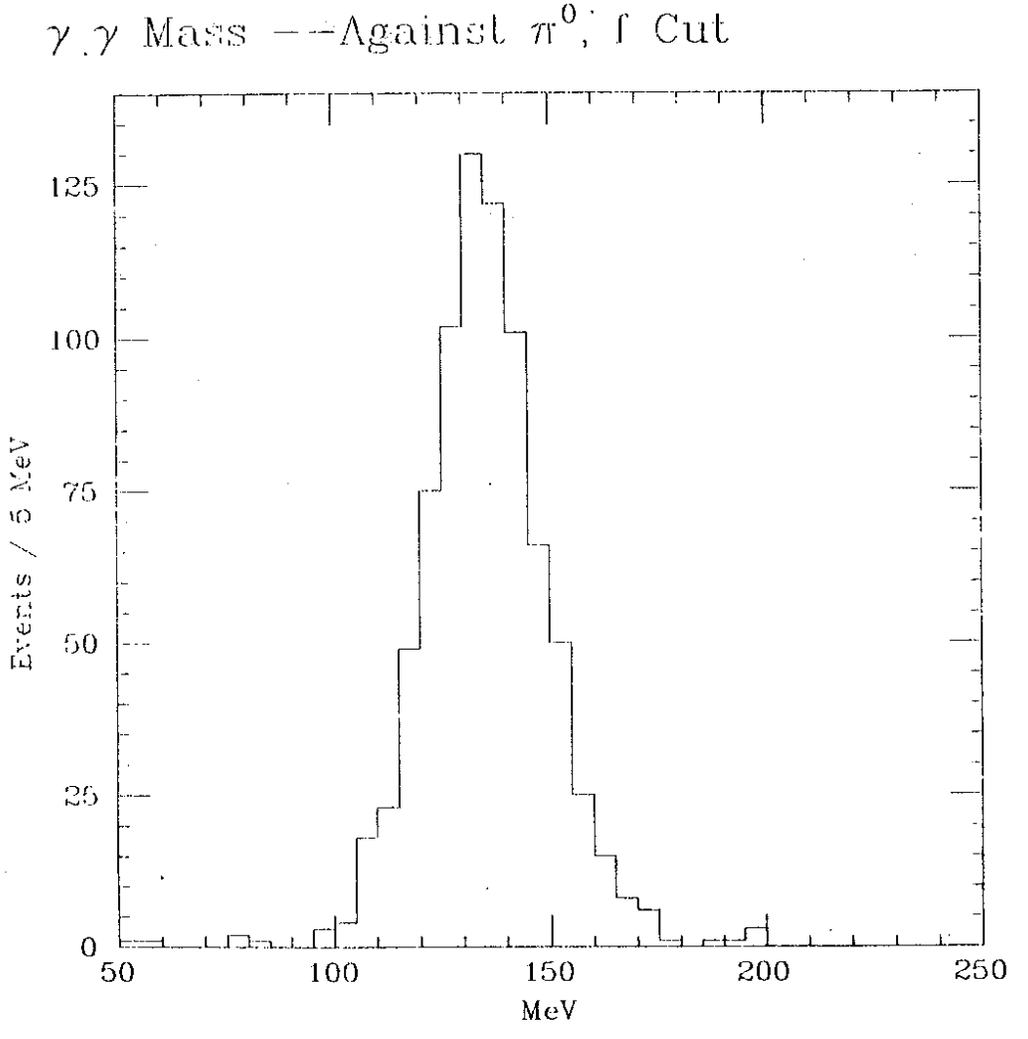

Fig. 19: $\gamma\gamma$ Effective mass distribution. Cuts as in Fig. 15

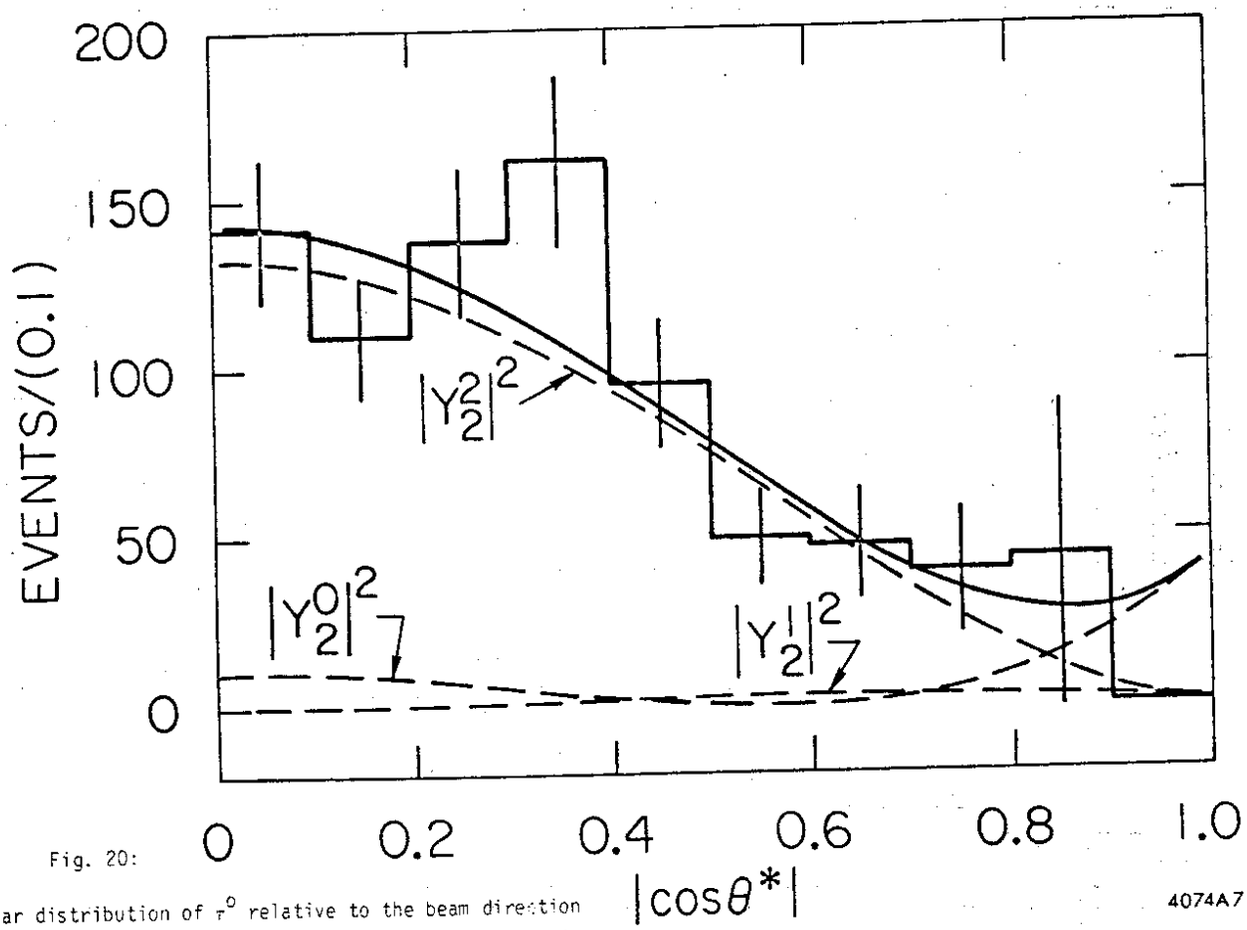

Fig. 20:

Angular distribution of π^0 relative to the beam direction in the f_0 rest frame. The fitted contributions of helicity 2, 1, 0 states are indicated

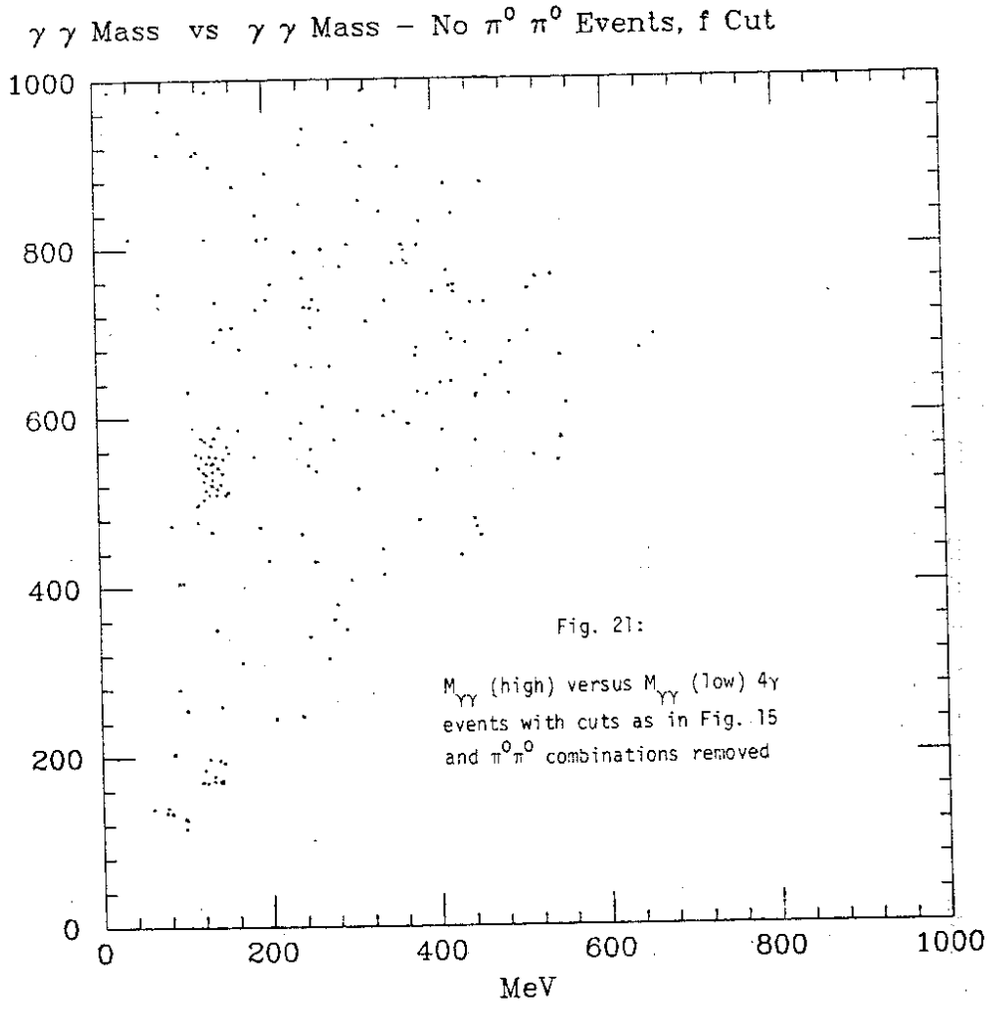

Fig. 21:

$M_{\gamma\gamma}$ (high) versus $M_{\gamma\gamma}$ (low) 4γ events with cuts as in Fig. 15 and $\pi^0\pi^0$ combinations removed

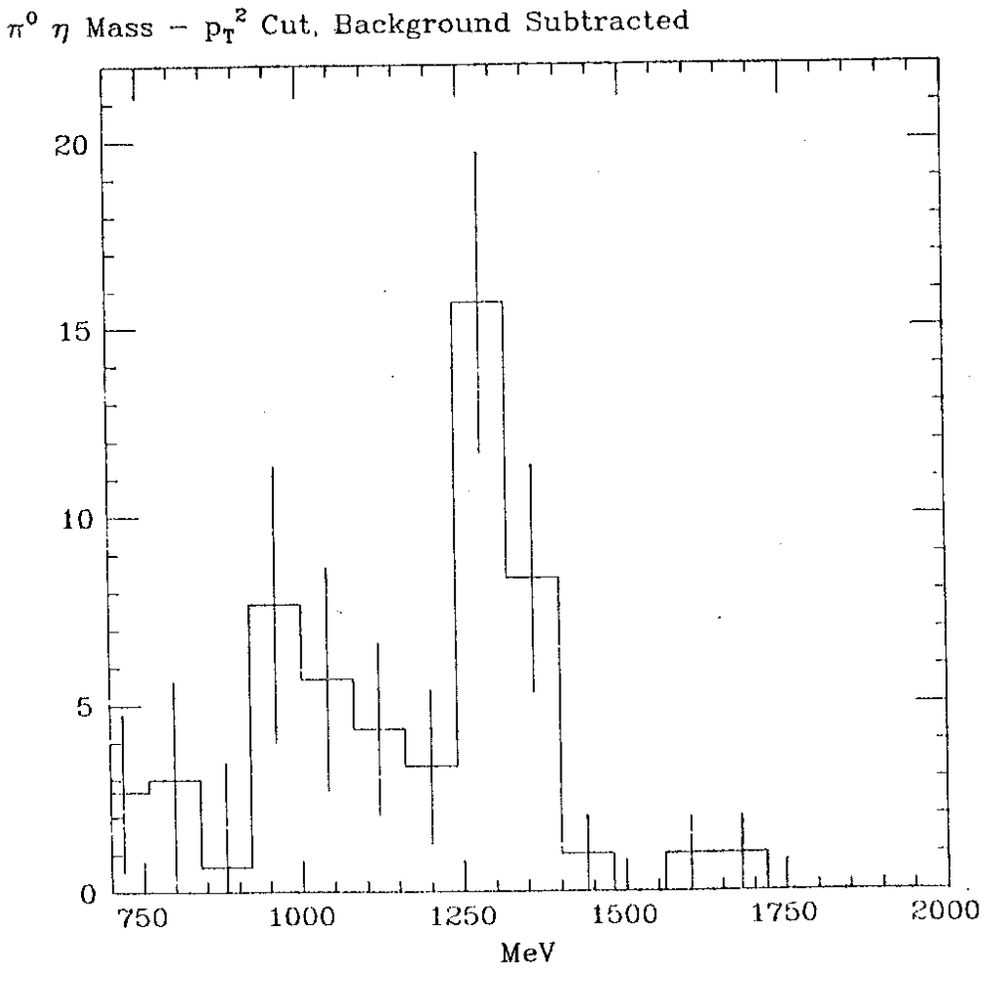

Fig. 22: Background subtracted $\pi^0\eta$ mass spectrum. Cuts as in Fig. 21

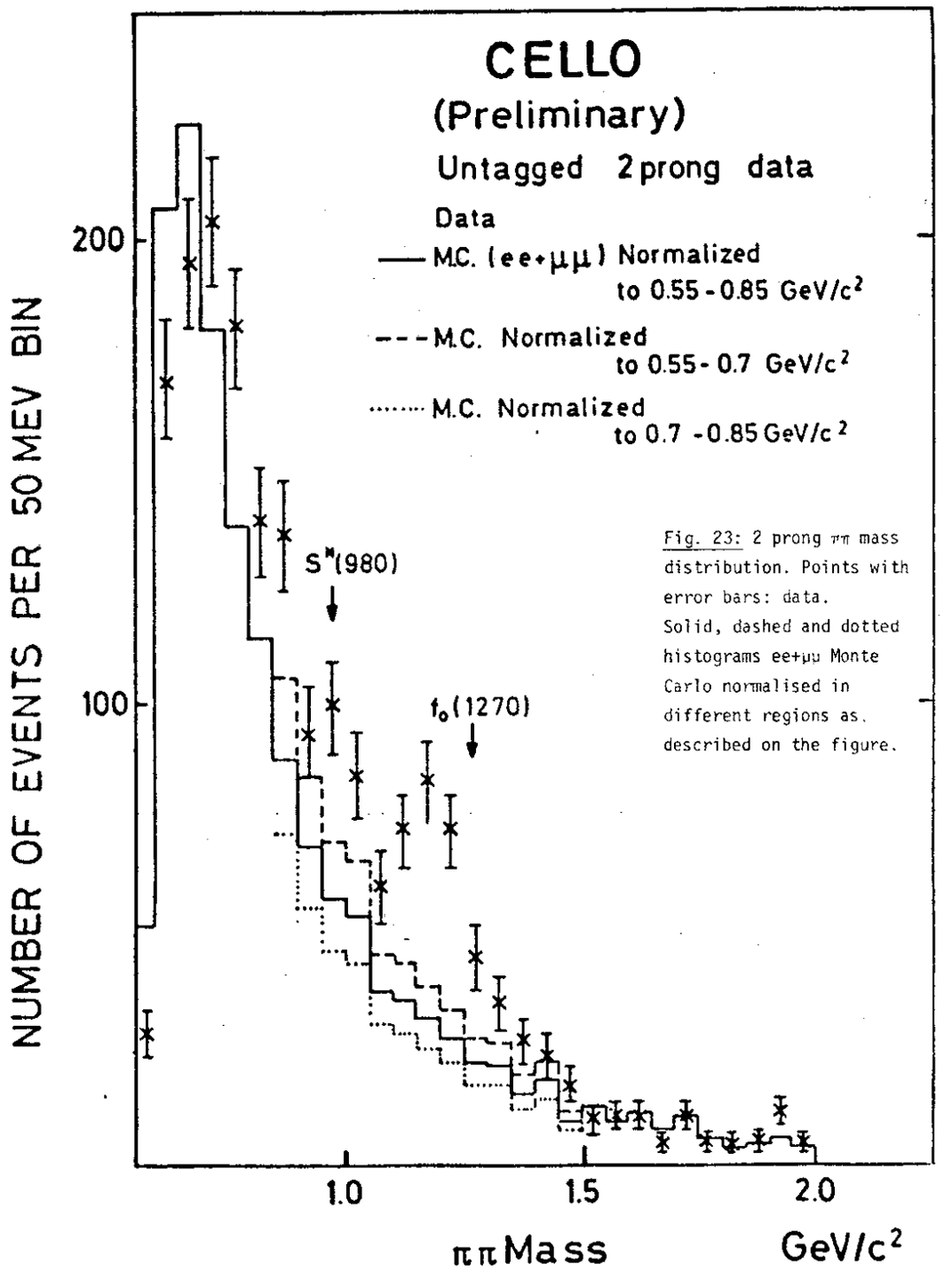

Fig. 23: 2 prong $\pi\pi$ mass distribution. Points with error bars: data. Solid, dashed and dotted histograms ee+μμ Monte Carlo normalised in different regions as described on the figure.

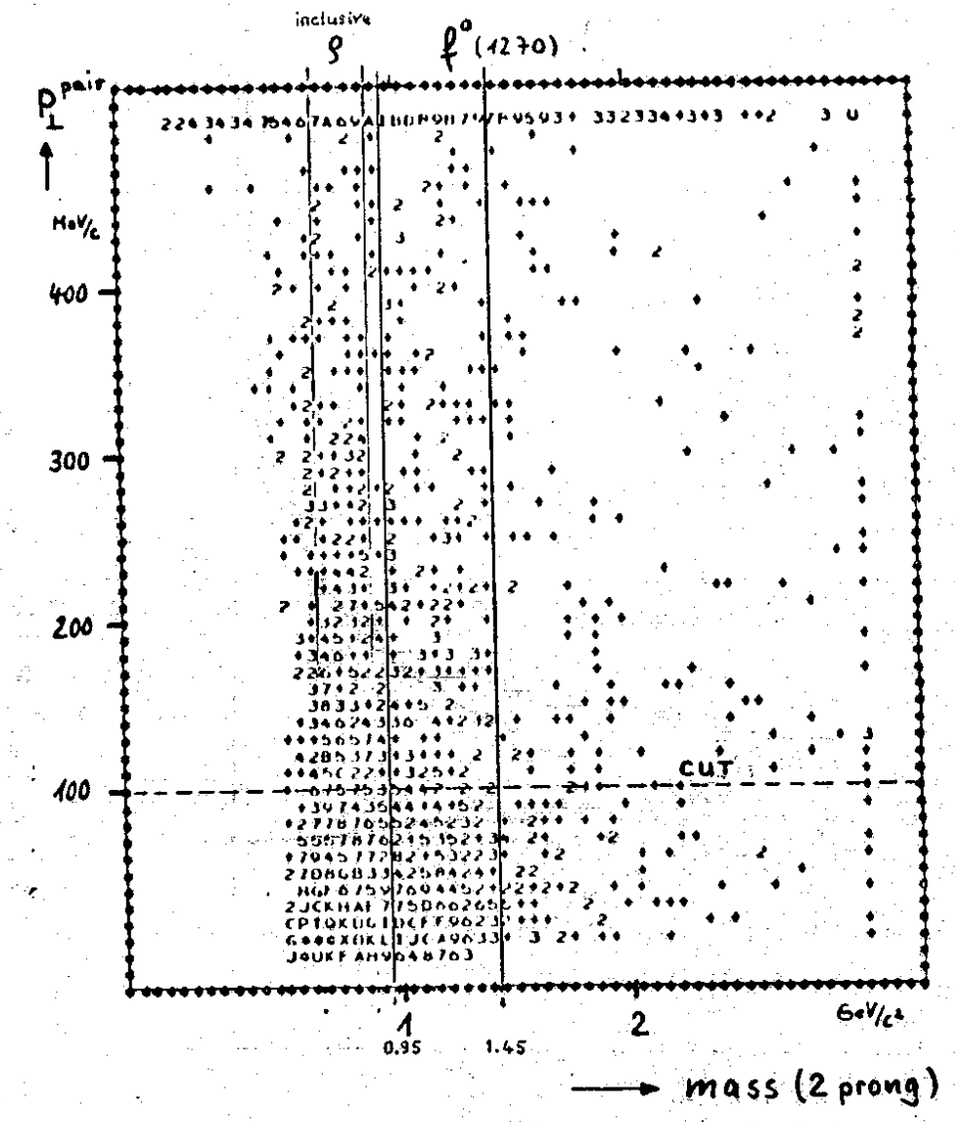

Fig. 24: $|\Sigma \vec{p}_T|$ versus ππ mass for 2 prongs

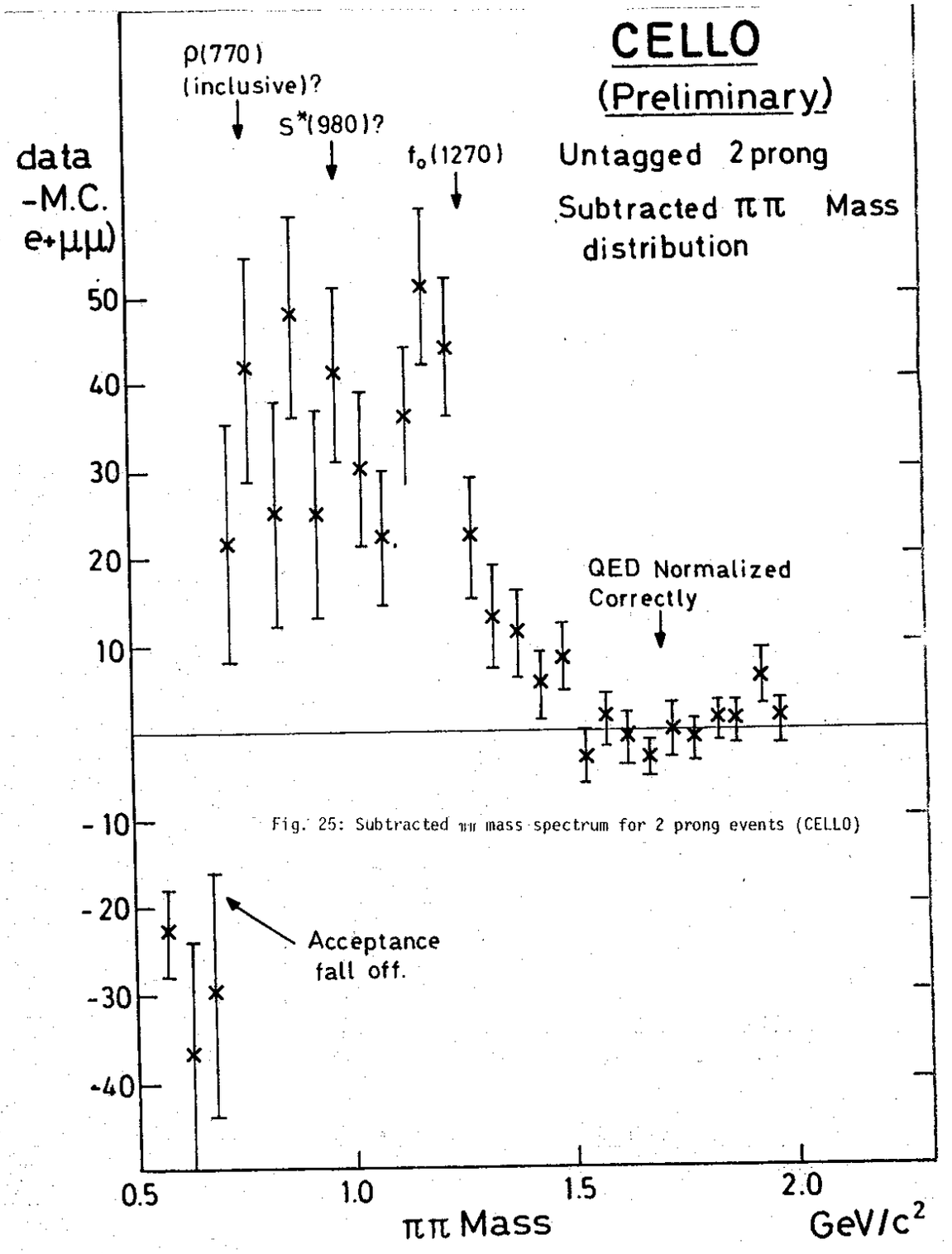

Fig. 25: Subtracted ππ mass spectrum for 2 prong events (CELLO)

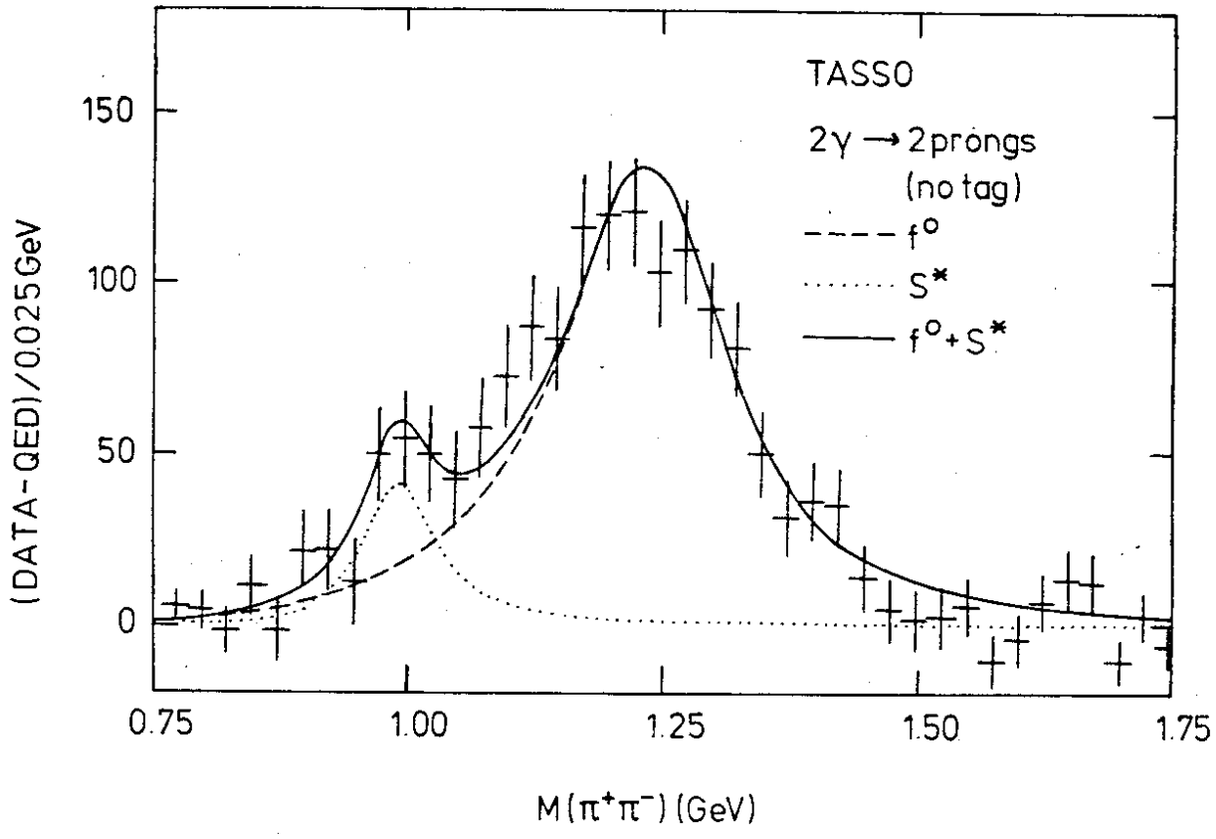

29.04.81

Fig. 27: Subtracted ππ mass spectrum for untagged 2 prong events (TASSO). Fits to f_0 and S^* using data book masses and widths are shown

32524

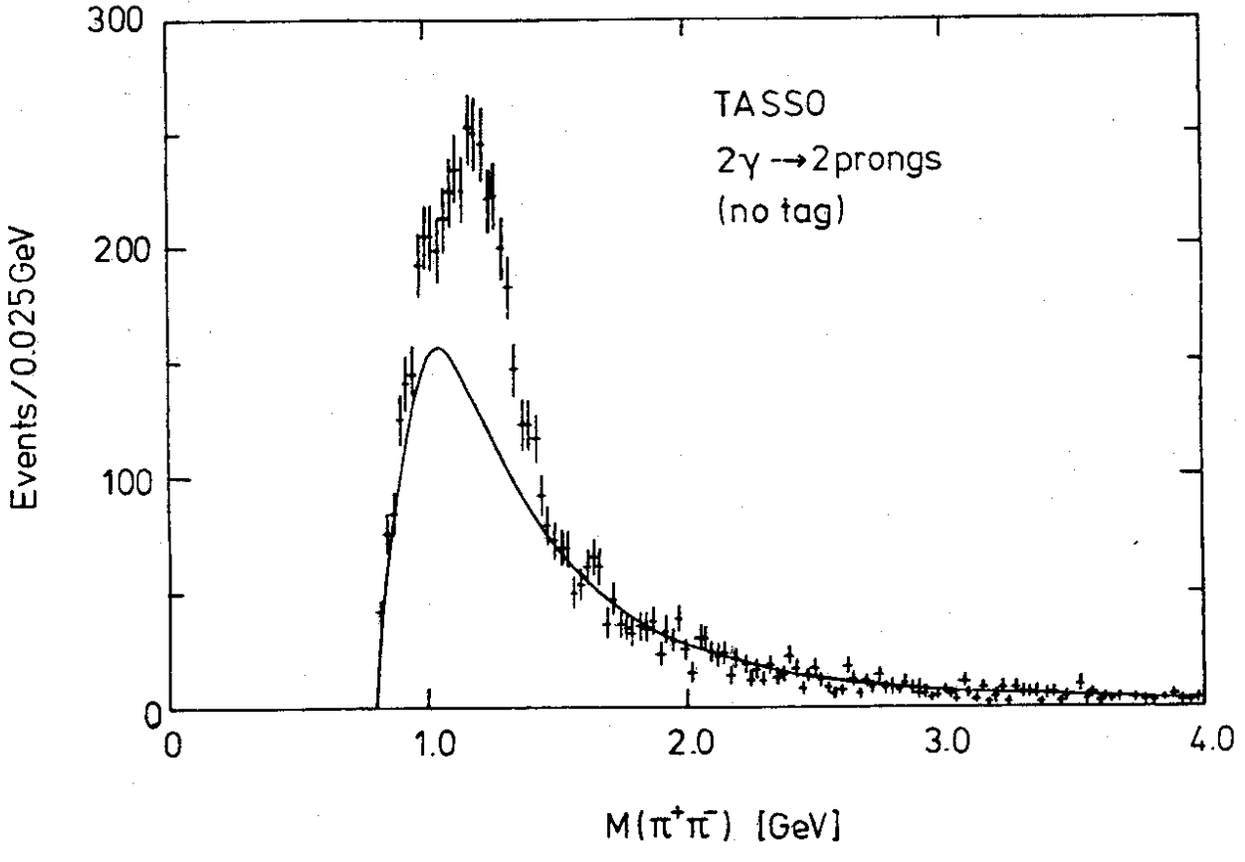

18.03.81

32420

Fig. 26: ππ mass spectrum for untagged 2 prong events (TASSO)

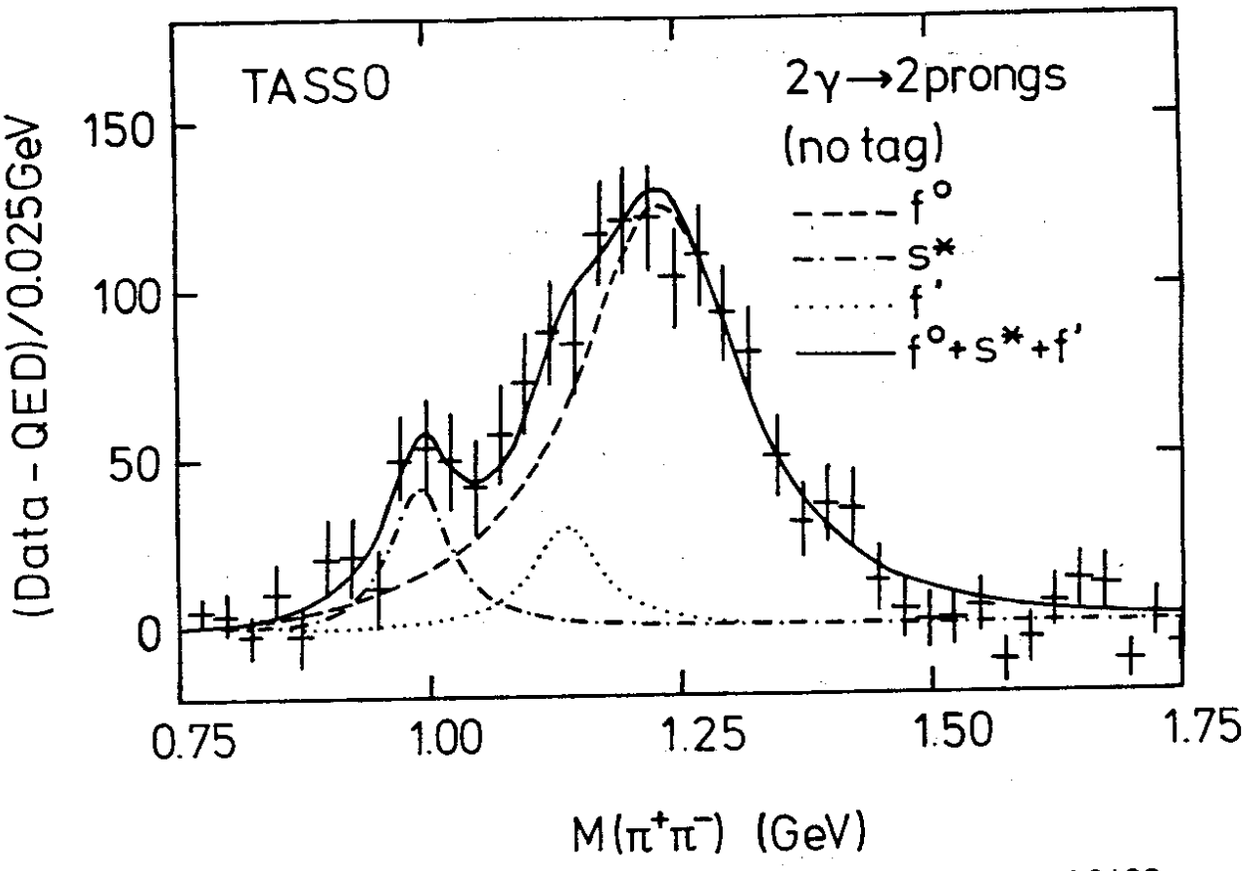

18.03.81

32423

Fig. 28: As Fig. 27 except fit contributions due to f_0, S^* and f' ($f' \to K^+K^-$) are shown

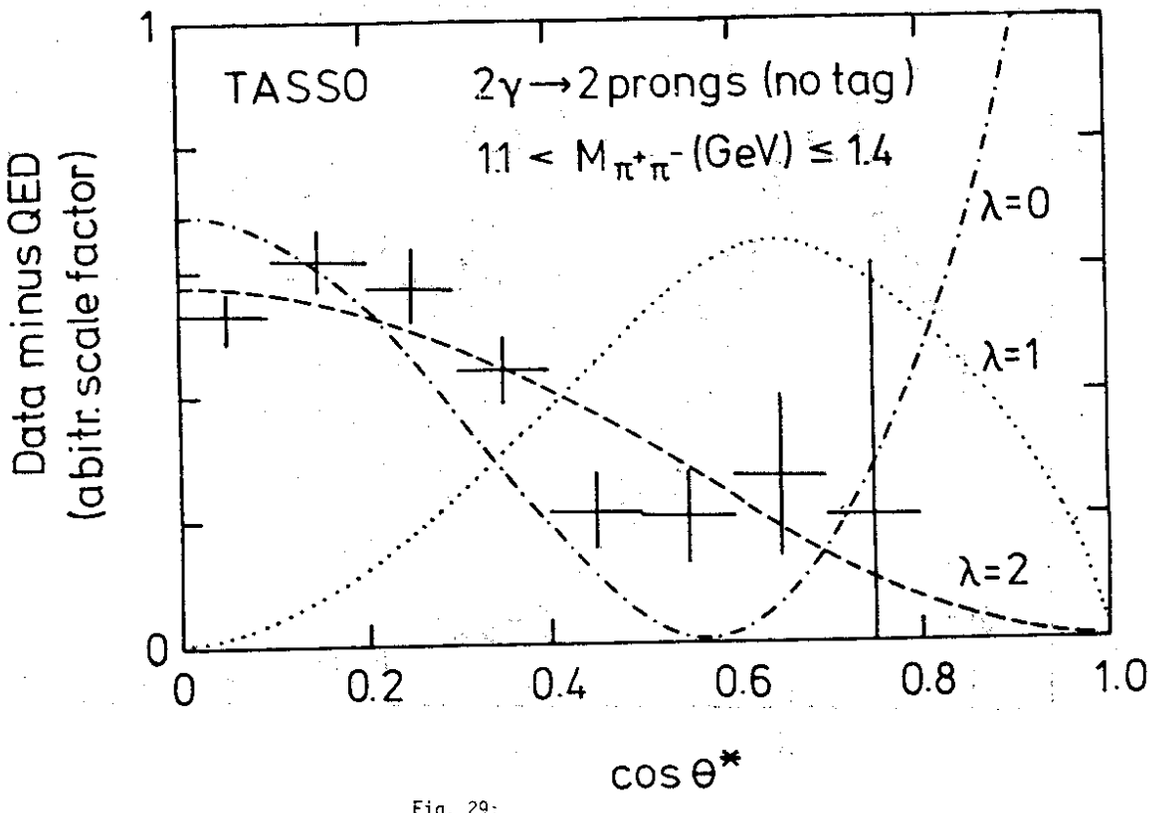

Fig. 29:

19.03.81

32422

Subtracted centre of mass decay distribution for the f_0 region: $1.1 < M_{+-} < 1.4$ GeV/c^2 (TASSO). The curves indicate the distributions expected for pure $\lambda = 0, 1, 2$ helicity states.

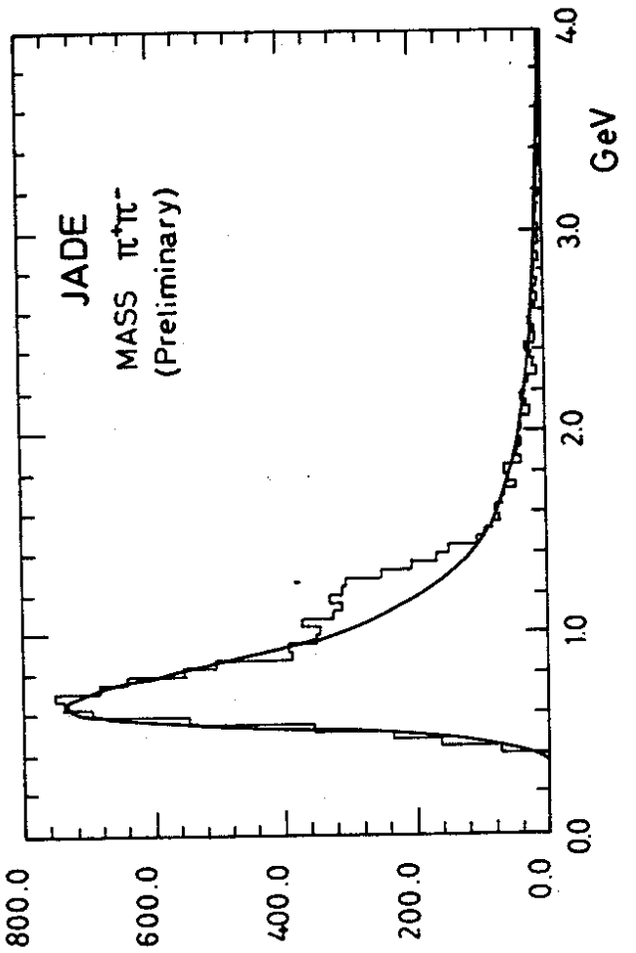

Fig. 31: Preliminary ππ mass spectrum for untagged 2 prong events (JADE)

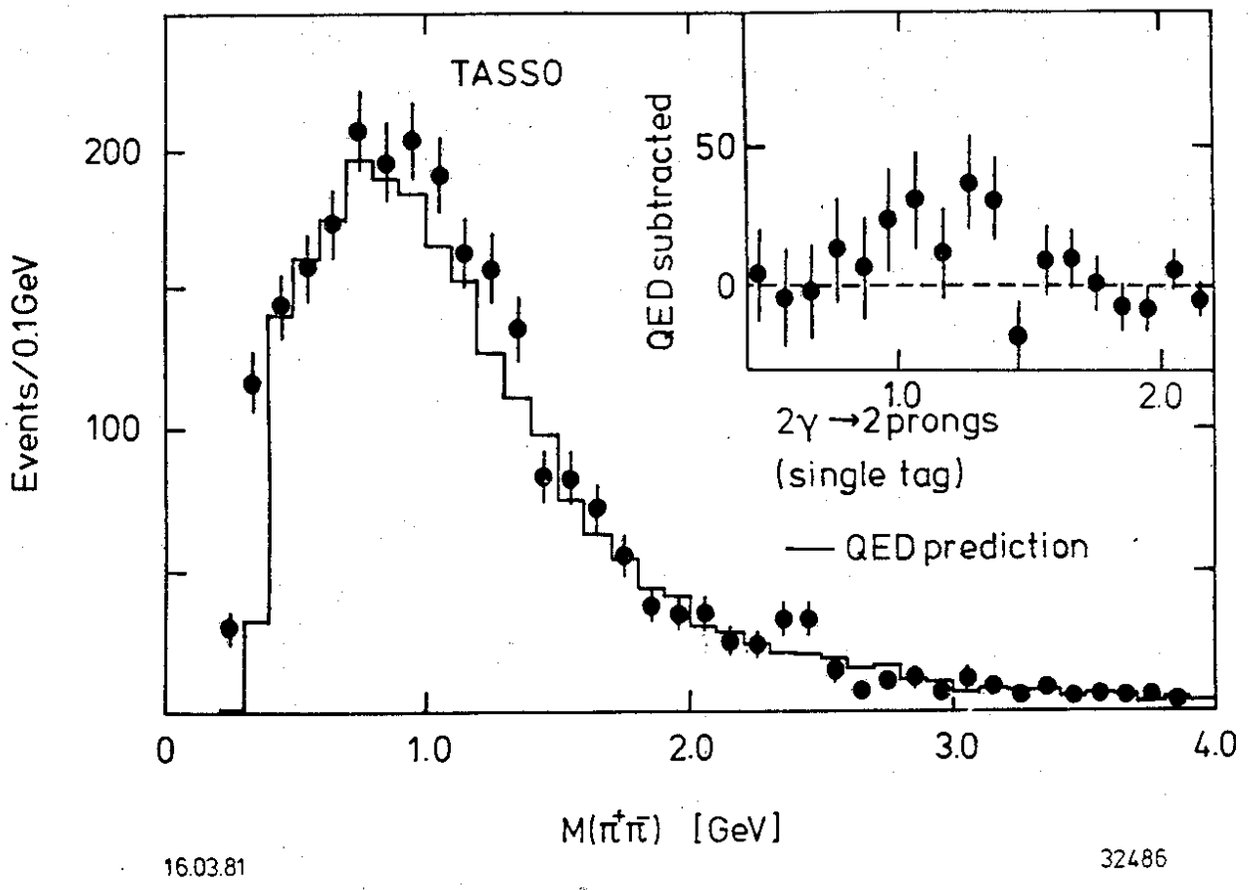

Fig. 30: ππ mass spectra for singly tagged 2 prong events (TASSO).
Main distribution: unsubtracted. Inset: subtracted.

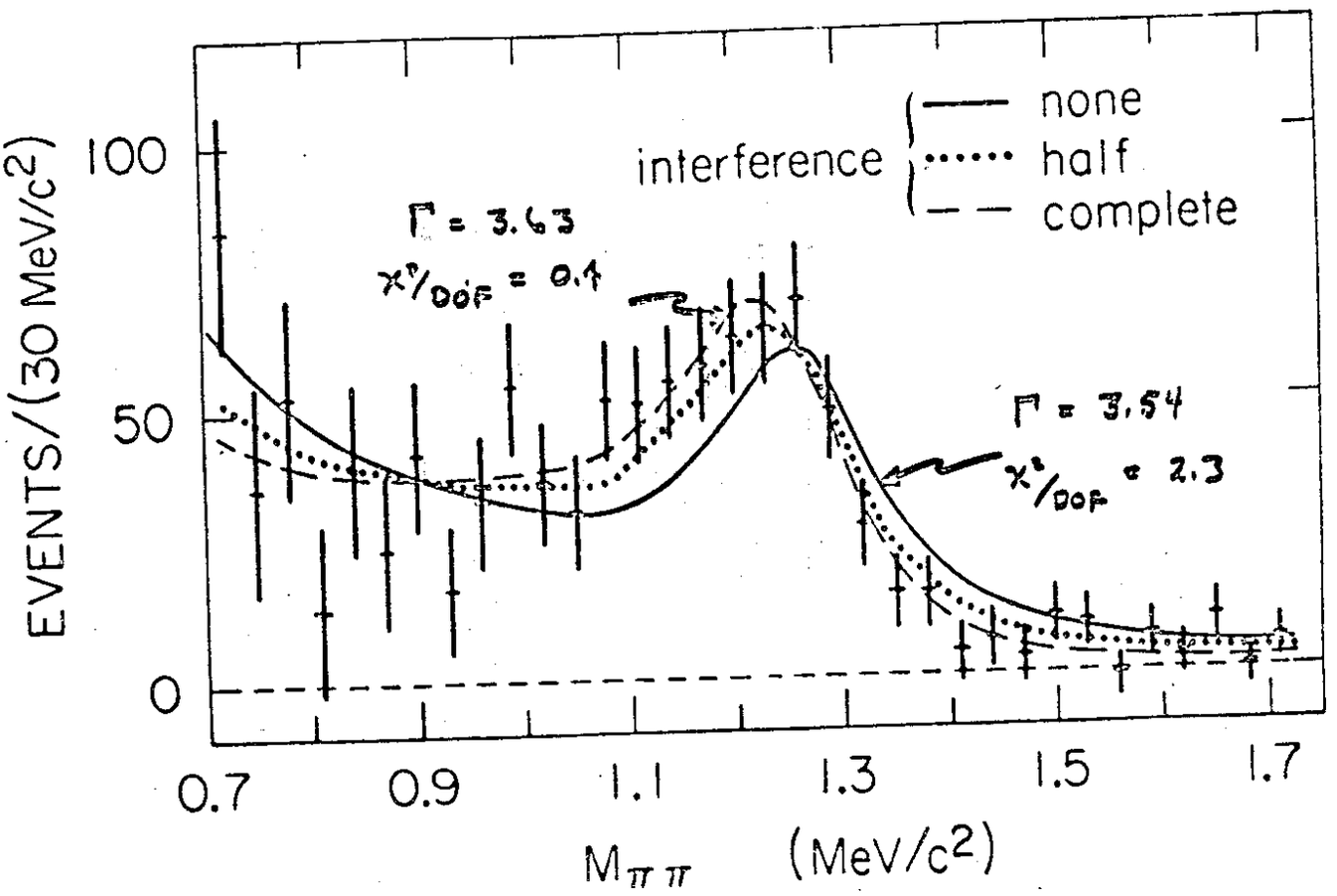

Fig. 32: ππ mass spectrum for untagged 2 prong events (MARK II). The effect of a ππ Born term interfering with the f_0 is shown

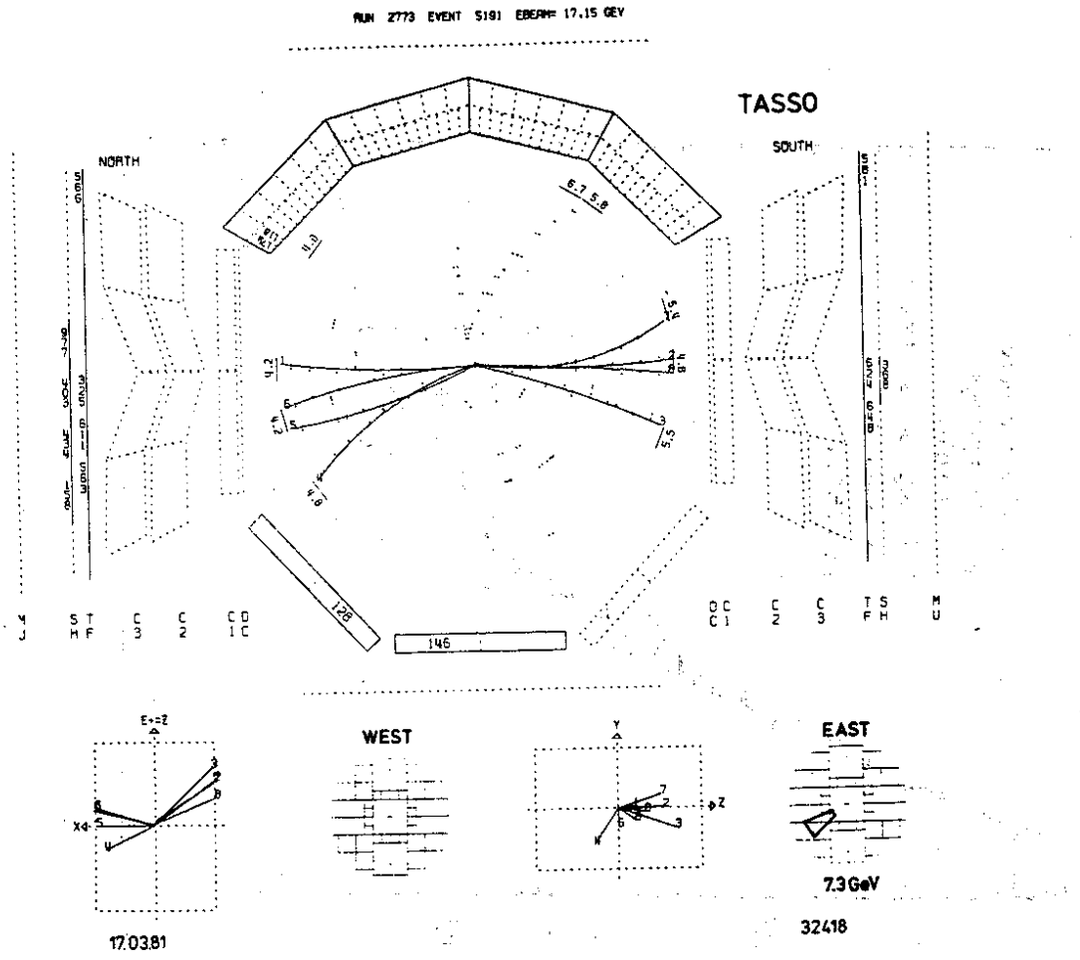

Fig. 33: A candidate event for the process ee→ee+2 jets with single tag

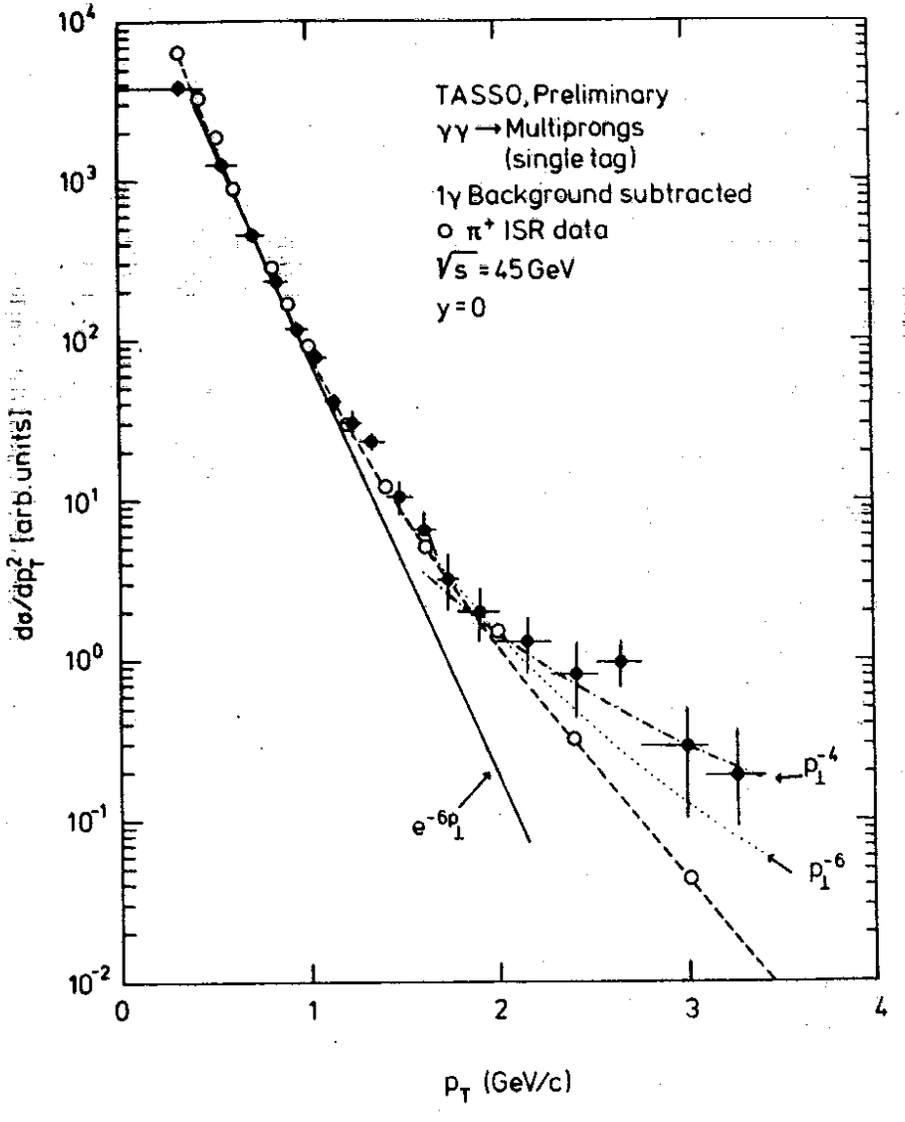

Fig. 34: $d\sigma/dp_T^2$ for $\gamma\gamma$-multihadron events (single tag) in comparison with ISR data (open circles)

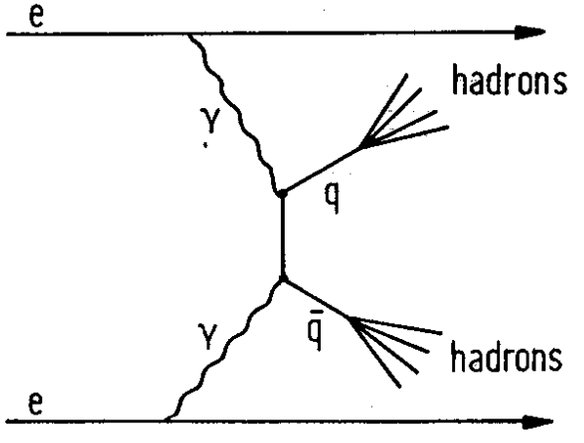

Fig. 35: Lowest order diagram giving 2 high p_T quark jets

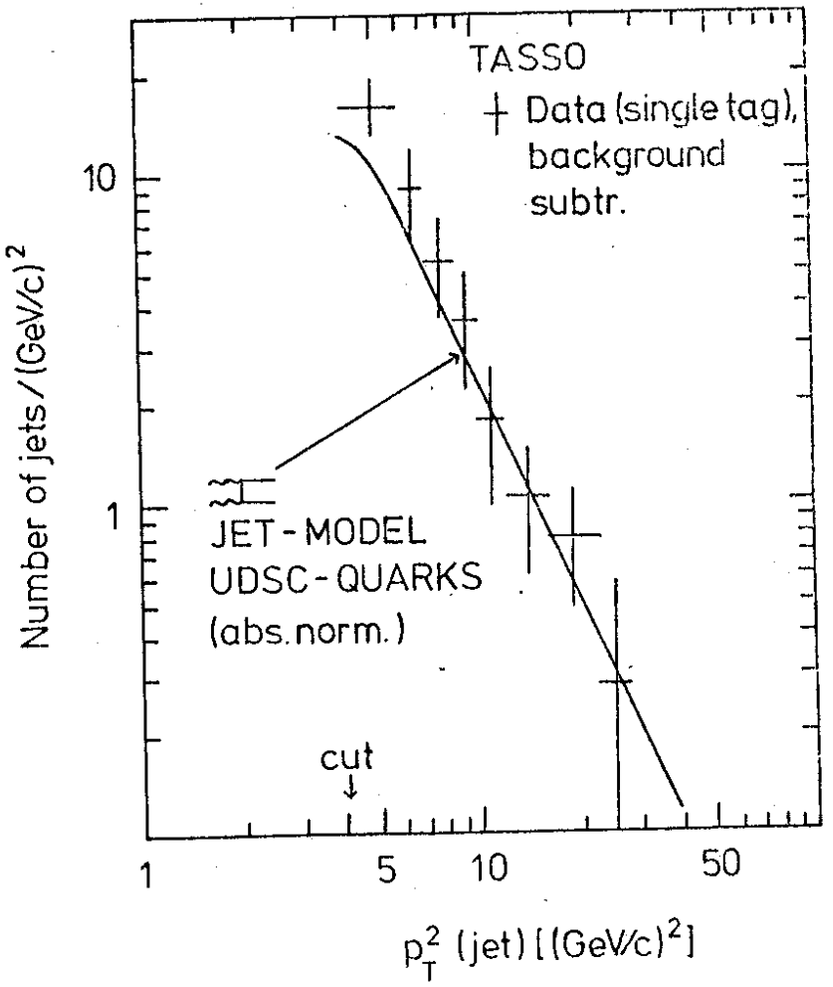

Fig. 36: p_T^2 distribution for 'jets' in single tag multihadron events. See text for the kinematic definition of a jet.

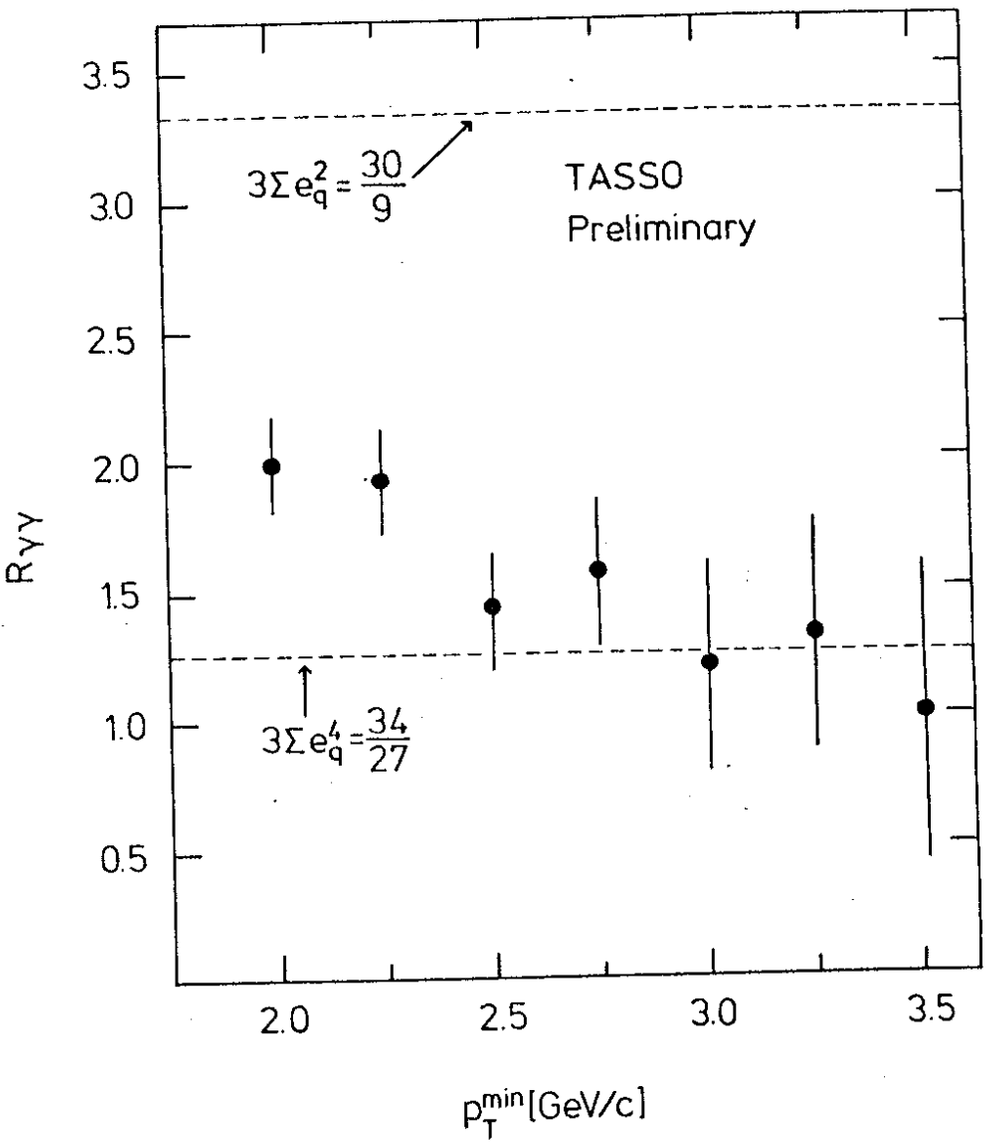

Fig. 37: Dependance of $R_{\gamma\gamma}$ on p_T^{MIN}(jet)